3D printing of solid polymer electrolytes by Fused Filament Fabrication: challenges towards in-space manufacturing

Félix Bourseau, Sylvie Grugeon, Ugo Lafont, Loïc Dupont

JPhys Energy

3D printing of solid polymer electrolytes by Fused Filament Fabrication: challenges towards in-space manufacturing

To cite this article before publication: Félix Bourseau *et al* 2023 *J. Phys. Energy* in press https://doi.org/10.1088/2515-7655/ad02be

3D printing of solid polymer electrolytes by Fused Filament Fabrication: Challenges towards in-space manufacturing

Félix Bourseau[1,2], Sylvie Grugeon[1,2], Ugo Lafont[3], Loïc Dupont[1,2,4*]

Laboratoire de Réactivité et de Chimie des Solides, UMR CNRS 7314, Hub de l'Energie, Université de Picardie Jules Verne, 15 rue Baudelocque, 80039, Amiens Cedex, France
[2] Réseau sur le Stockage Electrochimique de l'Energie (RS2E), FR CNRS 3459, Hub de l'Energie, 15 rue Baudelocque, 80039 Amiens Cedex, France
[3] European Space Research & Technology Centre Keplerlaan 1. 2201 AZ Noordwijk, The Netherlands
[4] Plateforme de Microscopie Electronique (PME) de l'Université de Picardie Jules Verne, Hub de l'Energie, 80000, Amiens, France
* Corresponding author: loic.dupont@u-picardie.fr

ABSTRACT

A new chapter of space exploration is opening with future long-duration space missions toward the Moon and Mars. In this context, the European Space Agency (ESA) is developing out-of-the-earth manufacturing abilities, to overcome the absence of regular supplies for astronauts' vital needs (food, health, housing, energy). Additive manufacturing is at the heart of this evolution because it allows the fabrication of tailorable and complex shapes, with a considerable ease of process. Fused Filament Fabrication (FFF), the most generalized 3D printing technique, has been integrated into the International Space Station (ISS) to produce polymer parts in microgravity. Filament deposition printing has also a key role to play in Li-ion battery (LIB) manufacturing. Indeed, it could reduce manufacturing cost & time, through one-shot printing of LIB, and improve battery performances with suitable 3D architectures. Thus, additive manufacturing via FFF of LIB in microgravity would open the way to In-Space Manufacturing (ISM) of energy storage devices. However, as liquid and volatile species are not compatible with a space station-confined environment, solvent-free 3D printing of polymer electrolytes is a necessary step to make battery printing in microgravity feasible. This is a challenging stage because of a strong opposition between the mechanical requirements of the feeding filament and electrochemical properties. Nowadays, polymer electrolyte manufacturing remains a hot topic and lots of strategies are currently being studied to overcome their poor ionic conductivity at room temperature. This work firstly gives a state of the art on the 3D printing of Li-ion batteries by FFF. Then, a summary of ionic conduction mechanisms in polymer electrolytes permits to understand the several strategies studied to enhance polymer electrolytes performances. Thanks to the confrontation with the specifications of FFF printing and the microgravity environment, polymer blends and composite electrolytes turn out to be the most suitable strategies to 3D print a lithium-ion polymer battery in microgravity.

KEYWORDS

3D printing, FFF, polymer electrolytes, Li-ion batteries, microgravity

INTRODUCTION

The launch of the Artemis program, in 2019, symbolizes the beginning of a new area in space exploration with targeted humans coming back to the Moon for a durable occupation (1). For the first time, astronauts will spend long-duration missions far from Earth without any regular resupply. Thus, it makes sense to manufacture tailorable devices in space, instead of shipping them through costly and time-consuming spaceship transports (2). That is why researchers, in collaboration with space agencies like the National Aeronautics and Space Administration (NASA) and the European Space Agency (ESA), are working on In-Space Manufacturing (ISM) methods and In-Situ Resource Utilization (ISRU)(3). The aim is to overcome this dependency, especially for vital needs such as food, energy, and protection against severe constraints of the space environment. Additive manufacturing methods are at the heart of this program as they enable fast fabrication of tailorable architectures with minimal material waste and low cost. Compared to traditional manufacturing methods, this consecutive layer's addition of materials on top of each other allows the precise building of objects with complex shapes. 3D printing has been intensively investigated for space applications (3) through the construction of space structures based on lunar or Martian regolith (4), spare parts fabrication, and food preparation(5) onboard space stations or on the Moon/Mars surfaces (2). "In-space" additive manufacturing breakthrough took place in 2014 with the first 3D printed polymer part by Fused Filament Fabrication (FFF), (also called Fused Deposition Modeling (FDM)) by NASA with the "3D printing in Zero-G" project (6). The first European 3D printer onboard the International Space Station (ISS) has been created, in 2016 by an Italian group, to 3D print polylactic acid (PLA) by FFF (7). The same year, ESA started to develop an FFF printer through the MELT project, to enhance the portfolio of polymers that could be used in such a peculiar environment focusing on polyether ether ketone (PEEK). This demonstration of the feasibility of 3D printing in microgravity has led to permanent installation of the Additive manufacturing facilities (AMF) onboard the ISS. Production of parts using other high-added value materials, like ceramics and metals, along with new printing techniques have been tested in simulated microgravity environment during parabolic flights demonstrating their compliance toward microgravity: metal 3D printing solutions by Force Metal Deposition (FMD) (8), Direct Energy Deposition (DED) or Electron Beam Fusion (EBF) and ceramic printing via VAT photopolymerization (8,9). The first automated on-orbit 3D printing of continuous carbon fiber-reinforced thermoplastics have been recently demonstrated by the Chinese Academy of Space Technology (10). Looking at additive manufacturing on the Moon or Mars, processing of regolith as a feedstock material using the Power Bed Fusion (PBF) technology was investigated (11).

Energy supply is a critical issue in space applications as it is one of the main causes of the space systems lifespan limitation. Energy mainly comes from solar power so rechargeable Li-ion batteries are used for all devices from the ISS primary power system to portable communications devices, going through life support systems (12). That is why batteries are key components that need a fast replacement in case of failure. Thus, the ability to manufacture tailorable energy storage devices is necessary for space exploration. Such capability fits the general strategy to decrease mission dependence from earth supply and will enable new maintenance strategy based on on-demand manufacturing instead of spare parts storage. Indeed, storage of spare parts is volume-consuming and shall be minimized specially in close environment like orbital station, lunar settlement of spacecraft for long travel toward Mars. It has been demonstrated that changing from spare part-based maintenance strategy toward on-demand in-space manufacturing will decrease by 78% the mass required for manufacturable set. (13)

With this in mind, Maurel and coworkers recently introduced the possibility of 3D printing batteries with Moon or Mars resources (12). They underlined the necessity to develop and optimize highly

resolution multi-material printers to 3D manufacture batteries out of the earth. The suitability of Na-ion devices instead of Li-ion has been highlighted due to the greater abundance of Na on the Moon and Mars (12). The crossbreed of the desired ability to manufacture tailorable batteries in space, and the knowledge acquired on FFF 3D printing in microgravity opens the way to lithium battery printing by FFF in a space station. Lithium-ion batteries (LIB) are known as the most efficient type of batteries (14). They are made of five parts: electrodes (cathode and anode), current collectors, electrolyte, separator, and casing. A gradient of potential induces a reversible movement of Li^+ through the electrolyte between hosting materials in electrodes: the rocking chair movement. Cathodes and anodes are composed of conductive materials to convey electrons, and active materials to allow movement and storage of Li^+ in their structure. Today's electrolytes are liquids containing organic solvents that enable fast motions of Li^+ between electrodes, while the separator forms a barrier for electrons to avoid short circuits. However, the microgravity environment impeaches the use of liquid electrolytes and the presence of volatile and flammable organic solvents is hazardous in the confined environment of a space station. Thus, the 3D printing of a polymer electrolyte is a necessary step to overcome these issues and to achieve one-shot printing of a full polymer battery without any post-treatment (Li-ion polymer battery). This paper will be focused on the 3D printing by FFF of a polymer electrolyte with main challenges and strategies. The first part will give a state of the art on what has been done so far towards the 3D printing of batteries by FFF. Then, ionic conduction mechanisms in polymers will be detailed to understand the landscape of strategies to achieve polymer electrolytes. The final part will highlight suitable strategies reported to meet the main challenge which is the 3D printing of an efficient polymer electrolyte compatible with a microgravity environment.

I. 3D printing of Lithium-ion Batteries (LIB)

Since the 1980s (15), additive manufacturing has been involved in a lot of domains (16) such as medicine (17), aerospace (3), transport, building construction, electronics, food, and energy(18). It consists in successive addition of materials layer to build a 3D dimensional object. This technology could produce complex geometries at a lower manufacturing cost and shorter time than any commercially available process. (19) Advantages, issues, and feature resolution of each additive manufacturing technology have been more widely detailed in dedicated papers (16,20). Today, they are gathering seven categories, according to the ASTM standard (21)[fig.1]. Among them, material extrusion printing is the most accessible technique to produce polymer parts.

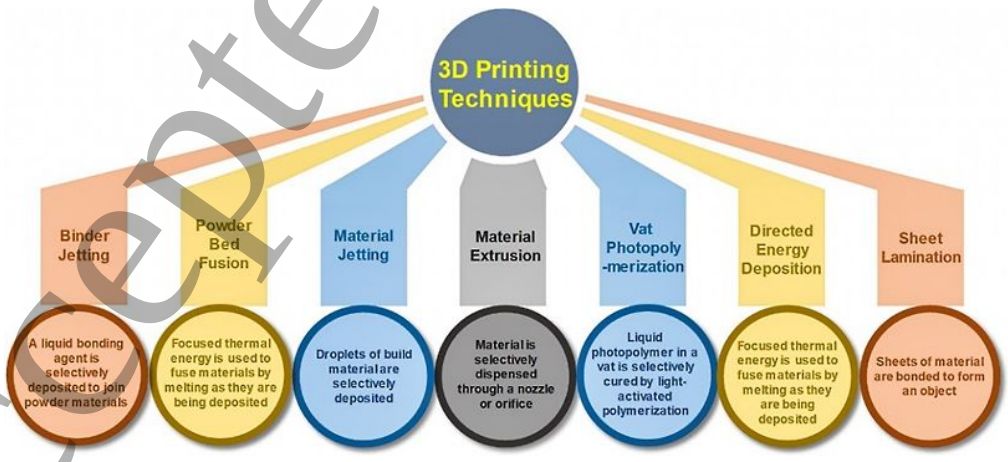

Figure 1 Additive manufacturing processes according to international ASTM standard Adapted with permission from (22)

1. Interests for LIB manufacturing

Since the 2010s, interest in the 3D printing of Li-ion batteries is growing because it can help to take up some manufacturing challenges (22): develop micro-energy storage devices and make energy storage manufacturing processes shorter, easier, and cheaper. The first pioneer industrials in this field, such as SAKUU, started to produce 3D-printed batteries. The breakthrough brought by additive manufacturing of Li-ion battery is the freedom of design which happens at three levels in **constructing strategies** (direct printing or methods with post-treatment), **electrode architecture** (surface pattern, thin film, 3D network or fiber), **and battery configurations** (sandwich, in-plane, concentric tubes or fiber) (23) [fig.2(a)]. Thus, it enables to:

- **Manufacture all-solid-state batteries with structural stability.** Indeed, each part of the battery is 3D printable in the solid phase to manufacture in one shot an all-solid-state battery. The intrinsic interlayer adhesion, which guarantees the mechanical integrity of printed parts, can provide a high interfacial adhesion between electrolytes and electrodes. That is why FFF has been studied, as a suitable method to create all-solid-state Li-ion polymer batteries in one-shot (24). In the case of Lithium-Metal Battery (LMB), Li metal anode printed by Direct Ink Writing (DIW) can limit dendrite growth thanks to a high specific area, periodic large porous structure, and high Li^+/electrons transports**.** (25)
- **Improve electrochemical performances.** 3D printing enables to optimize electrodes and electrolyte structures at macroscopic and microscopic scales. Electrodes can be manufactured with specific 3D pattern structures like zigzag lines, periodic micro lattice spirals, or circle grids (18,26). Simulations have shown these structures can give optimized 3D ionic diffusion pathways with shortened ion transport distances for a Li-ion polymer battery (27) [fig.2(b)]. It is also possible to play with electrodes and electrolyte thicknesses. Indeed, at same volume, interdigitated or in-plane battery configurations, mean larger surface areas with shorter ion transport distances. In these configurations thicker electrodes can be manufactured while preserving short ion transport distances [fig.2(c)]. **These tailorable designs contribute to increasing the power density**. High macro and micro porosity rates, induced by 3D printing processes and a specific design, facilitate ionic transport in liquid electrolytes through the free space of electrodes. It permits to create thicker electrodes without any limitation on power density (25). Thus, it allows the manufacturing of thicker electrodes with higher mass loadings **to obtain higher areal and volumetric energy densities.** Optimized structures permit to increase the areal active surface by maximizing the mass loading of active materials and controlling electrode thickness (23,28). Xueliang Sun's group has optimized the 3D electrode pattern to print a thick cathode of 1500 µm in order to achieve energy and power densities comparable to the reported performances of the LFP cathode (26). In interdigitated battery configuration, higher electrodes (higher number of layers) contribute to the rise in the areal capacity (29).

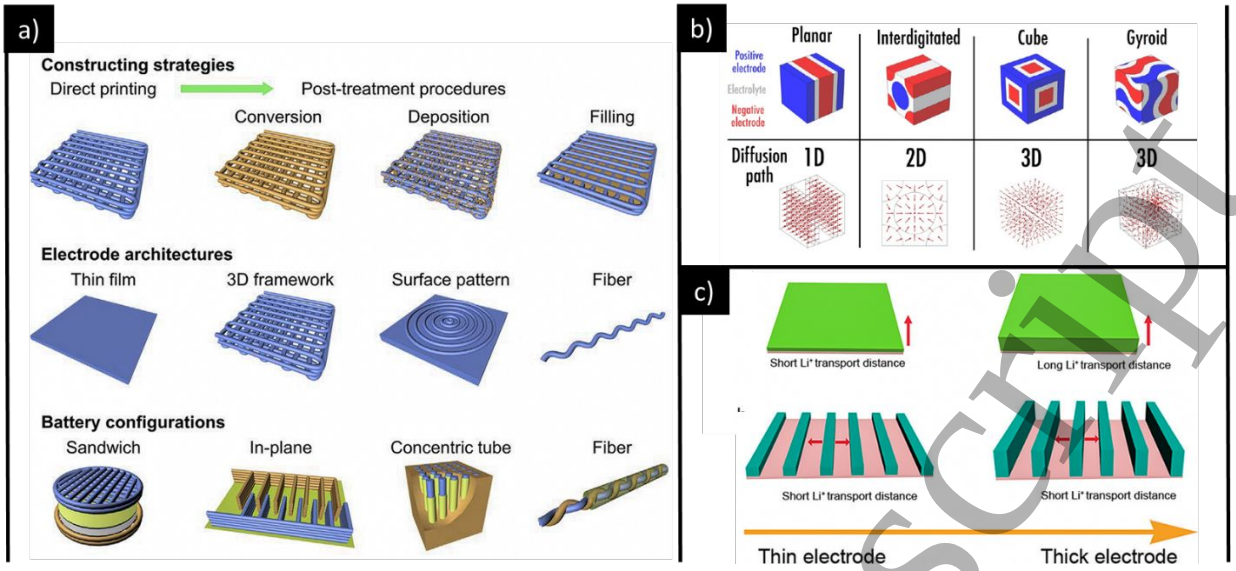

Figure 2 (a) 3D architectures perspectives at 3 levels Adapted with permission from (23) © 2020 Elsevier Inc, (b) Simulations of diffusion paths depending on electrodes 3D architecture adapted with permission from (27) © 2019 Springer Nature, (c) Towards smart free form-factor 3D printable batteries Adapted with permission from (26) © 2018 American Chemical society

- **Manufacture micron-sized batteries with customized shapes.** Micro batteries are more and more essential due to technological advances. Resolution of 3D printing in the range of micrometers (16) and tailor-made geometries open new horizons for integrated and flexible energy storage devices in portable technologies (30). For instance, the 3D micro battery of Ke Sun and coworkers(31) has been printed by DIW, with a nozzle of 30 µm. Quiming Chen *et al.* (32) have printed their Li-ion micro battery (7.6 x 3.8 x 3 mm) based on Gel Polymer Electrolyte (GPE) via stereolithography. The increase in volumetric energy density, brought by 3D printing, helps to create smaller batteries with comparable performances.

- **Lower manufacturing costs** thanks to a reduction of material wastage and production time savings compare to a conventional process. Indeed, the conventional battery manufacturing process is made of seven steps whereas battery 3D printing by FFF is composed of 2 steps: filament preparation and one-shot printing (23) [fig.3]. The use of a multi-materials printer can enhance the productivity by avoiding nozzle cleaning steps between each filament.

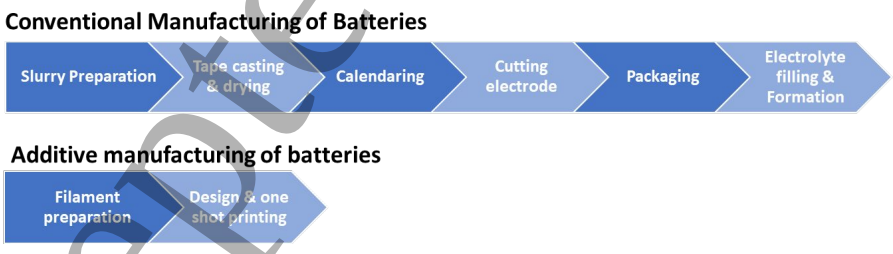

Figure 3 Comparison of conventional and additive manufacturing steps

Material Extrusion (ME) and vat photopolymerization are the two most studied 3D printing categories for energy storage devices manufacturing (25) due to their high versatility, low cost, and ease of process. ME technology consists in dropping off a melted thermoplastic polymer through a nozzle. The feedstock could be filament (**Fused Filament Fabrication, FFF**), ink (**Direct Ink Writing, DIW**), or pellets (**Fused Granulate Fabrication, FGF**). First reported papers on 3D printing for energy storage applications involved DIW because of its great adaptability to multi-material manufacturing and its

high resolution (1 to 250 µm). However, issues with ink rheological behavior have restricted its use (18). Vat photopolymerization also known as stereolithography (SLA) provides sub micrometers printing resolution. It consists in curing a photo resin thanks to the energy brought by a laser or UV light. However, it limits the choice of polymers to suitable photopolymers, and operations cost tends to be higher (29). Maurel *et al*. have reviewed main studies about energy devices 3D printing by ME (33). FFF turns out to be interesting as it provides good processability and the possibility of printing an entire battery in one-shot. Moreover, it requires a low-cost set-up, as well as it enables fast fabrication of a wide variety of polymers for relatively small parts. The main drawback is that this procedure suffers from a lower printing resolution (50-200 µm) than other techniques.

2. State of the art on FFF printing of LIB

In the FFF printing of LIBs, the feeding material is a filament composed of a thermoplastic polymer matrix, loaded with active and conductive materials necessary for the proper working of batteries. Thus, the 3D printing of an entire Li-ion battery requires 6 filaments corresponding to each part [fig.4]:

- **2 electrodes filaments** *(polymer + active & conductive materials)*
- **2 current collector filaments** *(polymer + conductive materials)*
- **1 filament for separator** *+ Liquid Electrolyte*
- **1 filament for the casing** *(high-performance polymer)*

Figure 4 Proof of concept of the Li-ion coin cell 3D printing by FFF with liquid electrolyte. Adapted with permission from (30). © 2018 American Chemical society

Filaments are composed of a thermoplastic polymer matrix blended with conductive materials (carbon black, carbon nanotubes (CNT) or carbon nanofibers (CNF)) for current collectors, with conductive and active materials (such as $LiFePO_4$ (LFP), $LiNi_xMn_yCo_zO_2$ (x+y+z=1) (NMC) for the cathode and $Li_4Ti_5O_{12}$ (LTO), graphite for the anode) for electrodes. As solvent free method, all of these materials are introduced under the shape of powder or pellets in an extruder. Inside, raw materials are melted and blended, thanks to screw rotation and heating, to obtain a viscous blend. The latter steps out through an extrusion die to create a 1.75mm diameter homogeneous filament. Conductive materials need to percolate to offer pathway for electrons, meanwhile active materials need to be accessible for Li cations. Thus, the viscosity, wetting coefficient and materials feeding modes (sequencing) are key parameters to reach a convenient morphology. Since 2017, several research groups have tried to achieve this concept (33). First papers were focused on introducing charges in polymer with low loadings to create composite thermoplastic filament for FFF. Commonly used polymers in 3D printing such as PLA or ABS were blended with graphene. Zhang *et al*.(34) as well as Foster *et al*. (35) studied 3D-printed graphene-based PLA negative electrodes(34,35). Their strategy was to limit the content of graphene to obtain a 3D printable filament (<30 wt% of active material) but obviously, filaments suffered from poor electrochemical performances. Between 2018 and 2022, 3 research groups tried to 3D print each part of the Li-ion battery: Reyes *et al.*(30) in the US, Ragones, Vinegrad *et al*. (36) in Israel, and Maurel *et al*.(37) in France [fig.5]. All of them have worked with PLA as the host polymer for their composite filaments, and they have tried to progressively increase the content of charges.

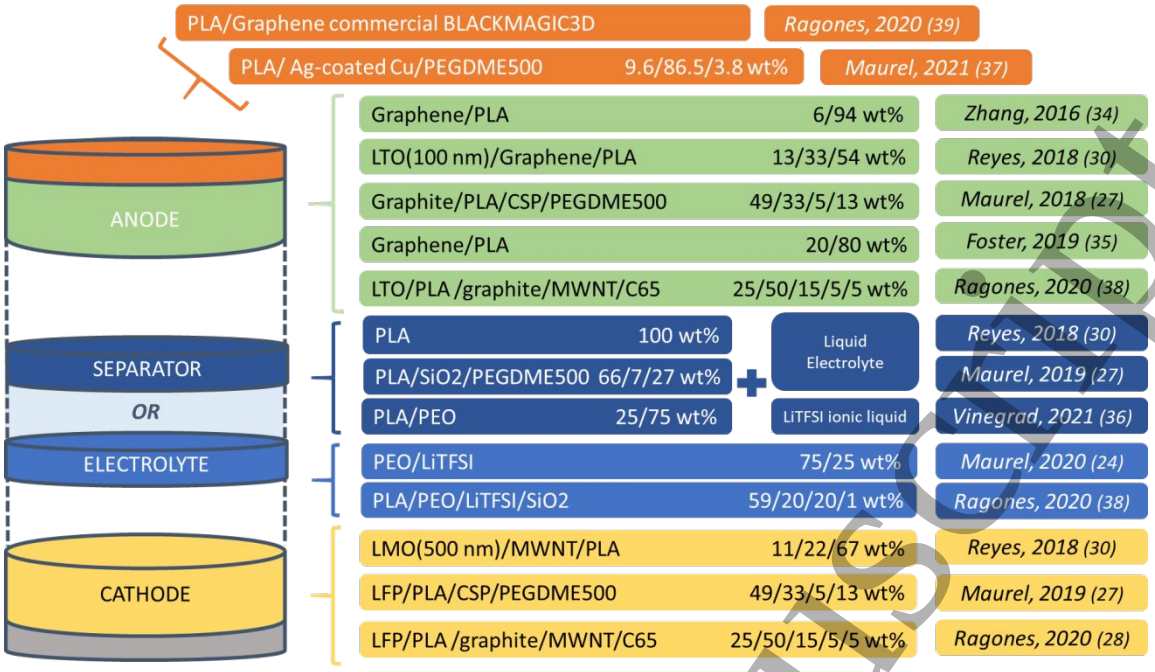

Figure 5 Reported studies on filaments for FFF 3D printing of Li-ion batteries

For the anode, Reyes, Ragones and coworkers have worked with LTO as active materials. They have succeeded in increasing the percentage of active materials in their filaments: PLA represents respectively 54 wt% and 50 wt% of the filament against 80 wt% for the graphene-based PLA from previous studies. Ragones group has played with carbons additives to enhance electrochemical performances by adding graphite, carbon black, and CNT. In the meantime, Maurel *et al.* succeeded in increasing the loading of active materials up to 49 wt% of graphite in their anode filament with only 33 wt% of PLA. They employed the plasticizer poly(ethylene glycol) dimethyl ether (PEGDME)500 to give more flexibility so as to be 3D printable. This strategy permits to obtain a reversible capacity of 200 $mAh.g^{-1}$ for a current density of 18. 6 $mA.g^{-1}$. The same strategy was applied to the cathode filament. LFP was chosen as active material by Maurel and Ragones groups and $LiMO_2$ (LMO) by Reyes and coworkers.

For electrolytes, two strategies have been considered: 3D printing a separator which must be impregnated with a liquid electrolyte, or 3D printing a polymer electrolyte (PE). Reyes *et al.* have printed and soaked a commercial filament of PLA with a liquid electrolyte whereas Ragones *et al.* tried to soak a polymer blend of PLA and poly(ethylene oxide) (PEO) with ionic liquid [fig.6]. Maurel *et al.* have 3D printed a composite filament of PLA with SiO_2 to improve the separator soaking ability. As for electrodes, they circumvented stiffness issues of the filament thanks to a plasticizer. These two latter groups have also worked on polymer electrolyte printing. Filaments were based on PEO-lithium bis(trifluoromethanesulfonyl)imide (LiTFSI) which is up to now the most studied and efficient single polymer-based electrolyte at temperatures above 60°C. At a lower range of temperature, it suffers from poor ionic conductivity (10^{-5} – 10^{-6} $S.cm^{-1}$). Moreover, LiTFSI has a plasticizer effect on PEO which turns out to be very difficult to print. The first possibility is to put less LiTFSI and to modify the 3D printer to be able to print a polymer electrolyte at the cost of electrochemical performances (24). Incorporating other materials to stiffen the filament is a second strategy which has been tested by Ragones *et al.* They have blended PEO/LiTFSI with PLA and SiO_2 to obtain a 3D printable filament. In both cases, printed electrolytes suffered from poor performances at lower temperatures and were still very difficult to 3D print. (36)

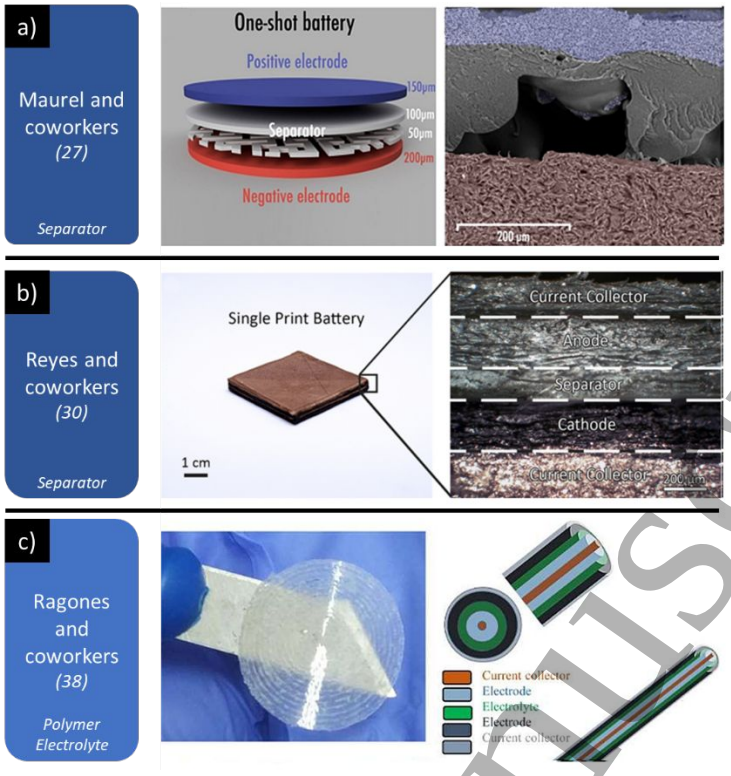

Figure 6 Reported proof of concept of 3D printed full Li-ion batteries by FFF (a) Adapted with permission from (27), ©2019 Nature Springer, (b) Adapted with permission from (30), © 2018 American Chemical society (c) Adapted with permission from (38), © Ragones 2019. Published by ECS.

Up to now, studies about 3D printing of liquid electrolyte batteries using FFF have been dedicated to proofs of concept. Replacing the liquid electrolyte with a printed polymer electrolyte is a critical step due to its poor mechanical behavior and its poor ionic conductivity at low temperatures (25°C). Thus, printing an electrolyte by FFF is the main challenge to successfully manufacture Li-ion polymer batteries. The following section will summarize ionic motion mechanism in polymer electrolyte and its key parameters.

II. Polymer electrolytes

Organic (polymers) and inorganic (ceramics) materials have been widely investigated to achieve solid electrolytes toward all-solid-state batteries(39). Polymers are easily processable and offer good interfacial properties for a low cost of material. Ceramics are more ionic conductive, confer more rigidity, and provide thermal and electrochemical stability(39). The first use of polymer materials as electrolytes in LMB was reported by Wright and Armand in the 1970s for safety concerns(40,41). More recently, the first commercialization of a polymer electrolyte happened with a system based on PEO and polyvinylidene fluoride (PVDF) for LMB made by the French industrial Bollore(42). Basic Polymer Electrolytes (PE) are made up of a single polymer matrix and a lithium salt. Polar groups on backbones dissolve lithium salt to allow the movement of Li^+. The following electrolyte properties are targeted (43):

- **High ionic conductivity:** to convey efficiently Li^+ between electrodes (10^{-3} $S.cm^{-1}$). It will impact high C-rate performances, specific capacity, and power density(44).
- **Electrochemical stability**: to remain stable and not be oxidized or reduced upon cycling.
- **High transference number (t_+):** to avoid polarization during cycling.
- **Sufficient mechanical behavior:** to be processable, not to crack during cycling, and to maintain good contact with electrodes(45).
- **Electronic insulator**: to avoid short circuits.
- **Ease of processing:** to ensure fast manufacturing and try to avoid hazardous solvent methods.

Even if polymers have been identified as good candidates to achieve solid flexible electrolytes, their poor ionic conductivity at lower temperatures than their melting point restricts their use. There is a strong contradiction between having solid-like mechanical behavior and reaching a high ionic conductivity. Thus, this section describes ionic motion mechanisms in polymers to understand strategies to improve Li^+ conductivity in polymers.

1. Ionic conductivity mechanisms

In organic liquid electrolytes, ionic motion happens via diffusion whereas in ceramics, ions move via crystal defects(46). Unlike these two cases, ionic transport mechanisms in polymers are not commonplace because they are influenced by many factors. Thus, a lot of researchers have dedicated their work to a better understanding of Li^+ movement through polymers(43,47). In basic systems, polymers can dissolve lithium salt through a polar functional group(48,49) [fig.7]. A Lewis complexation of ions (acid-base interactions) is possible thanks to heteroatoms (O, N, S) to form polymer salt complexes. This complexation ability is linked to the donor number and dielectric constant of the polymer(49). The bond's strength is determined for a particular cation by the electron pair donicity of the coordinating groups on the polymer chain(50). General electrostatic interactions (ion-dipole) and non-electrostatic interactions also contribute to ionic solvation(50). Polymer salt complexes are composed of **free anions**, **solvated cations,** and **aggregated ions**. Most polymers have a low dielectric constant which leads to increased ions aggregation, through long-range Coulomb forces, reducing the overall ionic conductivity(47,51). At a defined temperature, we can describe the passage of a current through a polymer electrolyte as a combined contribution of ionic migration over a potential gradient, ionic diffusion due to concentration gradient, and ionic convection due to electrolyte velocity [equation 1].

$$i = -F^2 \nabla U \sum_{i=-,+} u_i c_i - F \sum_{i=+,-} D_i \nabla c_i + Fv \sum_{i=+,-} c_i$$

F = Faraday's constant
$\mathbf{D_i}$ = diffusion coefficient
$\boldsymbol{v}$ = Electrolyte velocity
U = potential $\boldsymbol{c_i}$ = charge concentration
$\mathbf{u_i}$ = mobility of charged species

Equation 1 General equation of current through a polymer electrolyte

Considering a dilute system, without any concentration gradient and negligible electrolyte velocity, we obtain a form of Ohm's law which corresponds to the following Kohlrausch law with [equation 2].

$$\sigma = \sum_i n_i q_i \mu_i$$

$\boldsymbol{n_i}$ = number of free charges species
$\boldsymbol{q_i}$ = charge number
μ_i = mobility of charged species

Equation 2 General equation for ionic conductivity

$$R = \frac{\tau_s}{\tau_\sigma}$$

$\boldsymbol{\tau_s}$ = structural relaxation time
$\boldsymbol{\tau_\sigma}$ = conductivity relaxation time

Equation 3 Decoupling ratio

Polymers' semi-crystallinity makes ionic mobility difficult to understand. It could be split in two categories: **movements coupled with polymer chain mobility** (in amorphous regions, also called free volume theory(52)) and **movements decoupled from polymer chain mobility** (in crystalline parts also called ion-conduction)(14,47,52). Angel *et al.*(53) introduced a decoupling ratio between the structural and the conductivity relaxation time [equation 3]. Below the glass transition temperature, structural relaxation time is long, the decoupling ratio is high: there is no link between ionic conductivity and chain segmental mobility. On the opposite side, above the glass transition, the decoupling ratio is becoming smaller than one: the ionic conductivity occurs thanks to polymer segmental mobility.

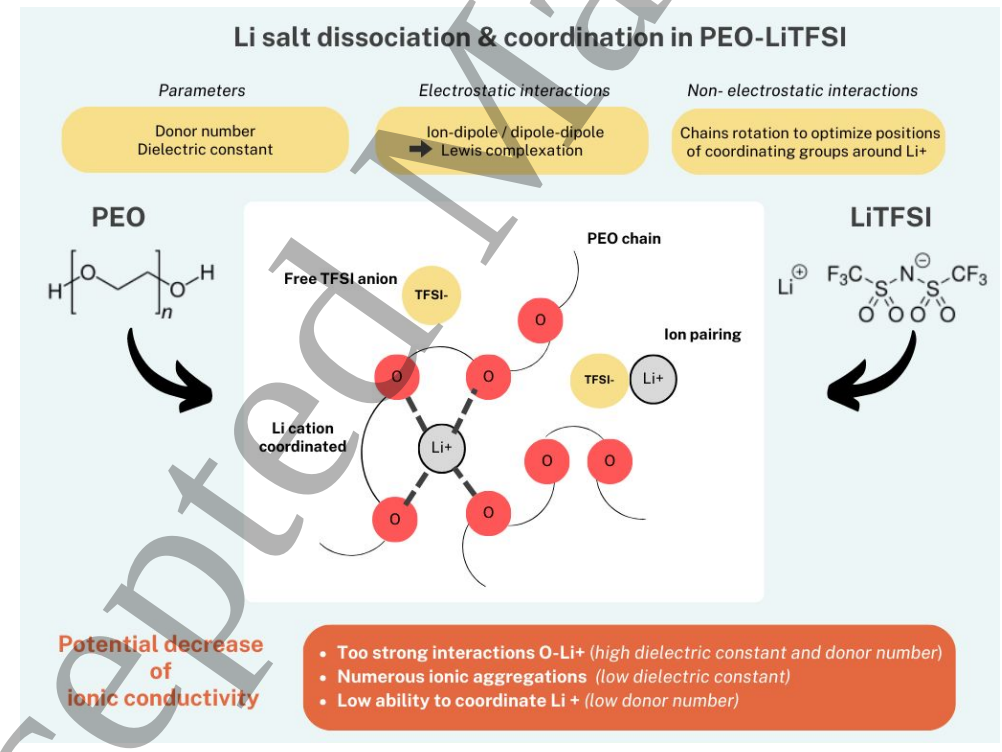

Figure 7 Salt dissociation and Li⁺ coordination in a PEO-LiTFSI system.

Thus, there are two main models for ionic transport in polymers in function of temperature: (49)

1) Arrhenius model (ion conduction): pathways are static so the ionic transport is decoupled from polymers chain mobility. It gives a good description of conduction in polymers below their glass transition temperature as well as in crystalline phases where the polymer chain's mobility is absent(54). Li^+ can move through vacancies offered by the crystalline structure. Folded chains form

a cylindrical tunnel for Li^+ to coordinate and be located inside this channel. Li-ion transport mainly depends on the tunnel structure formed by adjacent coordination sites(52). The conductivity increases with temperature by the activation process which enables Li^+ to move from one site to another. Geji *et al.* (55) have shown that Li^+ complexation by ether oxygen in crystalline region results in a coordination environment which is quite full. In these regions, there are no obvious static pathways for Li^+ movement. Thus, ionic movements occur preferentially in amorphous regions(56). However, Bruce *et al.* (57) have demonstrated that polymer crystalline structure can have better ionic conductivity than equivalent amorphous phase above the glass transition temperature, with a transference number close to unity.

$$\sigma = \sigma_0 \, exp\,(-\frac{E_a}{kT})$$

Equation 4 Arrhenius

$$\sigma = \sigma_0 \, T^{-\frac{1}{2}} \exp\,(-\frac{B}{T - T_0})$$

Equation 5 Vogel-Tammann-Fulcher (VTF)

2) Vogel-Tammann-Fulcher (VTF) model (free volume): ion pathways are dynamic so the ionic transport is coupled with polymer chains mobility. It gives a good description of conduction in polymers above the glass transition temperature and fully amorphous polymers where the segmental mobility is high. It corresponds to the free volume theory in which diffusion can occur when diffusing particles move from one free volume space to another(39). Conductive materials relax more rapidly than non-conductive ones, which means that ionic motion and segmental relaxation of polymers are linked (50). Daniel T. Hallinan and coworkers (43) considered two types of mechanisms:
   - **Segmental motion of the chains surrounding the lithium salt.** In the case of a PEO-LiTFSI electrolyte, Li^+ surrounded by six ether oxygens is the minimum free energy configuration(43). Segmental motion leads to the modification of configurations and enables Li^+ to move toward sites of lower free energy(43). It provides more chances for ions to perform faster migration. Ionic jumping can take place on the same polymer's chains (**intrachain ionic jumping**) or can occur between two different chains (**interchain ionic jumping**)(58).
   - **Diffusion of the entire polymer chain with coordinated ions**, **also known as vehicular transfer**(43). It can only occur for low molecular weight polymers (less than 2,000 $g.mol^{-1}$). It can explain the dependence of the ionic conductivity of polymers on their low molecular weight seen in the literature(43).

In both cases, Li^+ motion is due to stronger interactions of cations than anions with ether oxygens(51). However, free volume theory is limited in the case of semi-crystalline systems, incomplete salt dissociation, and glass transition temperature variation due to charge species(51). An enhancement of ionic conductivity at elevated temperatures is visible due to an increase in segmental motion, lower energy barriers for ion transport, and an increase in ion mobility and concentration(52). Maurel *et al.* (24) illustrated such a behavior experimentally for a 3D printed electrolyte PEO:LiTFSI (O:Li = 20:1) system by coupling differential scanning calorimetry (DSC) and ionic conductivity data. To summarize, 3 main behaviors of ionic conductivity *vs.* temperature can be identified: 1°/Arrhenius for crystalline systems, 2°/ VTF for amorphous systems, 3°/ Arrhenius and VTF mix for semi-crystalline systems(39).

Other groups tried to model Li^+ movement in different ways and at different scales. At a microscopic scale, the **Dynamic Bond Percolation (DBP)**(59) permits to describe ionic conductivity over a wide range of temperatures(47,60). Ion motion is described as a first-order chemical kinetics. The probability to find a Li^+ at a site *i* at the time *t* is $P_i(t)$ and W is the hopping rate from site *i* to site *j*. In the Arrhenius case, W=0 if the jump is forbidden, and W=1 if the jump is allowed [equation 6]. In a VTF case, W depends on the time because segmental motion can make jump forbidden or allowed during a certain amount of time called the renewal time. In this model, the diffusion coefficient is proportional

to the average renewal rate which is the rate at which a motion pathway between two sites becomes feasible(60). Even if it is one of the best models for understanding ionic conduction in polymers, it does not consider inertial dynamics and interionic interactions(60). Reducing the renewal time (by increasing segmental mobility) and reducing ion pairing (by increasing the dielectric constant) will increase overall ionic conductivity(47).

$$\frac{dP_i}{dt}(t) = \sum_j (-W_{ij}P_i + W_{ji}P_j), \quad \textbf{(a)} \quad W_{ij} = \begin{cases} 0, \text{ probability } 1-f \\ w, \text{ probability } f. \end{cases} \quad \textbf{(b)} \quad w = w(t).$$

Equation 6 Dynamic Percolation Bonding (DPB) with W the hopping rate (a) in Arrhenius case, (b) in VTF case

Quantum mechanics can also explain Li^+ motions in models in which Li^+ motion is described as a wavelength λ_{Li+} [fig. 8] (54). According to Zhou *et al.*(54), core factors for improving ionic conductivity are freer Li^+ and longer hopping distances with lower barriers between 2 coordinating sites. Adam and Gibbs(51) attempted to extend the theory of free volume. In their approach, transport occurs by group cooperative rearrangements rather than by hole-hole jumping motion. Ionic conductivity models for heterogenous systems are more complicated.

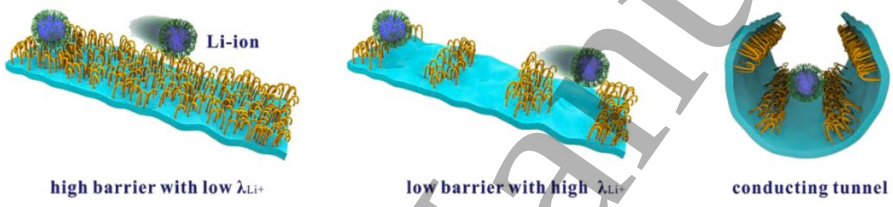

Figure 8 Schematic wave fluctuation mechanism of Li-ion migration in different SPEs (54)

According to (47), there are three ways to increase ionic conductivity at room temperature in polymers:

- Increase the number of mobile ions (adding Li salt) to increase the prefactor σ_0 in Arrhenius and VTF model [equations 4 and 5].
- Increase segmental mobility (decrease T_g and crystallinity rate) = make VTF mechanism effective at room temperature
- Decoupling from the segmental structure motion: create a structure in which Li^+ can move through static pathways = favor the Arrhenius mechanism
    - Polymer as an inactive support binder for percolating conductive materials
    - Polymer-in-salt strategies(61)
    - Composite with low crystallinity at the interface which creates pathways
    - Hard polymers: polymers which are less dense and thus, have a higher free volume(47)

The following figure summarizes main concepts of ionic transport in a homogeneous system of polymer and lithium salt [fig. 9].

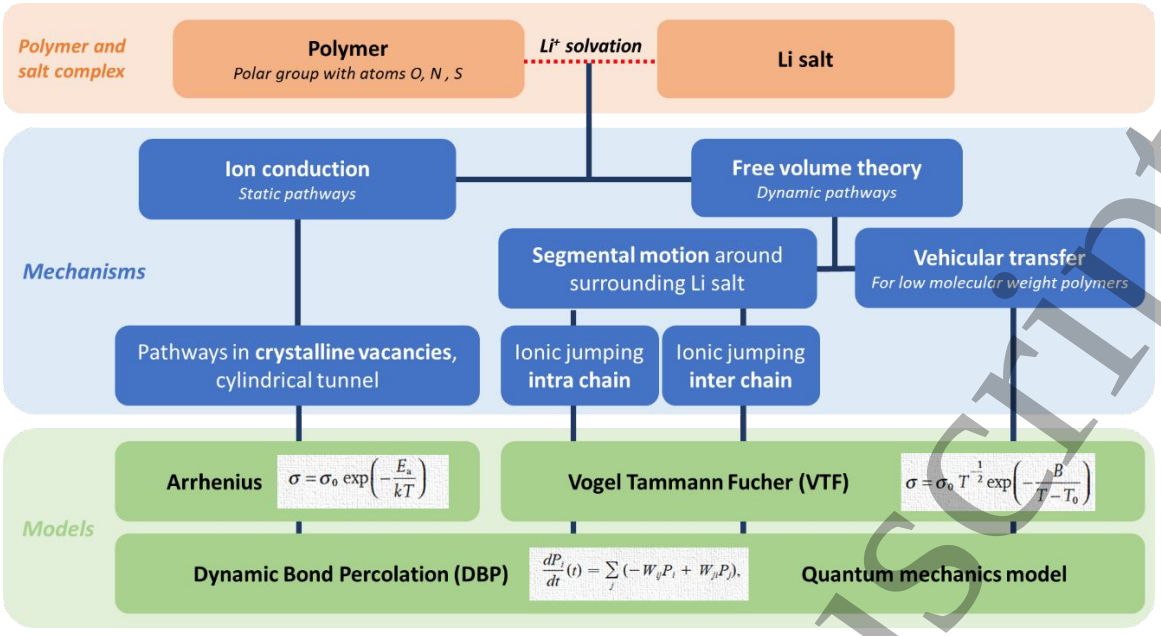

Figure 9 Main mechanisms and models of ionic conduction in a polymer electrolyte

2. Key parameters to improve the ionic conductivity

Main parameters influencing the above-mentioned ionic mechanisms are : dielectric constant and donor number, polymer structure and molecular weight, temperature, electrolyte architecture, or concentration of Li salt (52).

Dielectric constant and donor number influence the polymer solvation ability. Indeed, isolated electrons of polar groups must coordinate with Li^+ through Coulomb interactions to dissolve ionic salt. (51). Dolle *et al.* (49) provide the donor number and the dielectric constant for seven polymer matrixes depending on their polar functional group. They experimentally showcased that polymer affinity is dominated by the donor number. Ether, ester, and carbonate polymers seem to have good properties at 25°C. A high dielectric constant permits to reduce ion pairing and increase overall conductivity(50). According to Nan Meng and co coworkers (48), 4 main polar groups display a good ability to dissolve ionic salts: ether group (PEO, poly(ethylene glycol) (PEG), poly(vinyl acetal) (PVA), carbonyl group (poly(vinyl carbonate) (PVC), poly(propylene carbonate)(PPC), poly(methyl methacrylate) (PMMA)), nitrile group (polyacrylonitrile (PAN)), and fluorine group (poly(vinylidene fluoride)(PVDF)). The polymer solvation ability is a question of balance: with high dielectric constant and donor number, the ionic conductivity is limited by too strong chemical interactions between Li^+ and polar groups which reduce the segmental chains motion. In the opposite case, the ionic conductivity is decreased because dissociation of Li salt does not happen.

Polymer structure influences the ionic conductivity through the **segmental relaxation** of polymers chains. In high molecular weight polymer electrolytes, ion mobility is inversely proportional to the relaxation time (43). According to Nan Meng (48), this mainly relies on polymers' flexibility, inter and intramolecular forces, and crystallinity rate. Polymers' flexibility is linked to backbones and side chains structures. PEO backbones (C-O-C) have a high chain flexibility(58) whereas heterocycles such as poly(vinyl formal) (PVFM) or poly(vinyl butyral) (PVB) provide higher rigidity(48). In amorphous regions, segmental motion is highly increased. Thus, in a semi-crystalline polymer, ionic transport happens in amorphous regions (51,58,62). The low **crystallinity rate** in polymers is due to the macromolecular structures, simple, ordered, or symmetrical(48). This crystallinity could be decreased

by the introduction of fillers, other polymers, or plasticizers. Polymer structures also influence the polymer solvation ability which depends on the **steric position** of these polymers' groups(48). Devaux and coworkers (63) have shown that end groups own higher mobility than middle segments. It can play a key role in ionic interactions, depending on the **end groups chemical composition**. In the case of low molecular weight PEO, the hydroxyl group can solvate Li^+ which reduces polymer chain mobility. Finally, as described in the previous section, low **molecular weight polymer** can increase ionic conductivity thanks to the vehicular transfer mechanism. For PEO-LiTFSI at 76°C, this increase in conductivity is experimentally visible for a molecular weight lower than 2,000 g/mol (43).

Li salt concentration effect depends on the kind of polymer. In the case of poly(ethylene carbonate) (PEC), the addition of lithium salt improves the ionic conductivity. In the case of PEO, an increase in the lithium salt molar ratio improves the ionic conductivity until a threshold(39). When it is jumped over, undissolved lithium salt acts as a barrier for the motion of Li^+ which leads to a decrease in ionic conductivity. Increasing ionic salt concentration also reduces the polymer chain mobility because of chemical interactions between the heteroatom of the polymer and lithium salt. These two competing phenomena have been illustrated by Hallinan and co-workers in their review (43). The amount of lithium salt has also an impact on the micromechanical behavior by acting as a plasticizer. It reduces the crystallinity rate of the polymer while degrading the mechanical stability. Thus, there is an optimized lithium salt content, to reach an optimal conductivity without degrading the mechanical stability. For a homogeneous polymer electrolyte (PEO:LiTFSI), the best conductivity is reached for around O:Li = 10:1. However, in this basic homogenous system, a molar ratio of 20:1 is usually used to maintain a sufficient mechanical behavior. In polymers with low dielectric constant, ion-pairing occurs at low salt concentrations, while larger ionic aggregates (most of which are charged) form at higher concentrations (50). Thus, conduction mechanisms should consider the possible exchange of cations and anions between pairs and clusters (50). Ionic motion can happen by jumping from one ionic cluster to another one but also reduce chain segmental mobility. However, the t_+ number strongly goes down with salt concentration increase for the polyether systems such as PEO (64).

Electrolyte architecture has a fundamental role to play in ionic conductivity. In heterogeneous media, Bouchet *et al.* (65) have shown that the tortuosity of Li^+ pathways reduces the ionic conductivity. In their polystyrene (PS)-based block copolymer PS-PEO-PS, low molecular weight PEO increases excluded zone proportion (nonconductive zones in PEO near PS sides). Thus, a combination of higher molecular weight PEO and higher volume fraction of the conducting phase (PEO-LiTFSI) contributes to decrease the tortuosity in a block copolymer. In the model proposed by Carman [Equation 7], the conductivity of the composite is the bulk conductivity of the conductive phase (σ_0) multiplied by its volume fraction (ε) (which depends on excluded zones length λ). The tortuosity is represented by the factor τ (depending on the volume fraction of conducting phase ε and larger than 1). $1/\tau$ is the fraction of conducting volume that has the same transport efficiency as the bulk electrolyte. A percolation threshold of PEO cylinders may exist around 60 wt% of PEO that could explain the conductivity gap at room temperature from $6x10^{-7}$ S.cm^{-1} to $2x10^{-5}$ S.cm^{-1} for an increase from 36 to 74 wt% of PEO (65).

$$\boldsymbol{\sigma} = \frac{\boldsymbol{\sigma_0} \times \boldsymbol{\varepsilon}(\boldsymbol{\lambda})}{\boldsymbol{\tau}(\boldsymbol{\varepsilon})}$$

Equation 7 Carman-based model of ionic conductivity in a composite electrolyte(65)

In the case of composite electrolytes (polymer matrix + inorganic fillers), high fillers loadings can increase the tortuous lithium-ion path which can decrease the overall conductivity (52). The specific structure of "hard polymers", which can contain a greater internal free volume than soft polymers, can

offer new static pathways via Arrhenius conducting mechanism (57). This is the case of polydimethylsiloxane (PDMS) which has been used to improve ionic conductivity thanks to its high internal free volume (66). Thus, the aims for future polymer electrolytes are to decrease the crystallinity rate of the polymer matrix, maximize the Li salt molar ratio, and construct continuous fast ion paths (52).

3. PEO-LiTFSI polymer electrolyte

Since Armand and Wright's works on polymer electrolytes, the mix of PEO and LiTFSI has been the most studied single polymer-based electrolyte. A promising polymer for electrolytes should have the following characteristics: 1) functional groups with sufficient electron-donating power to form coordinated bonds with cations 2) suitable distances between such coordinating centers to permit the formation of multiple interpolymer-ion bonds 3) low barriers to the rotation for atoms in the main chain to ensure high flexibility so good segmental relaxation (50). PEO has a strong ability to dissociate and coordinate LiTFSI (48). It has the highest reported lithium salt solvating ability due to its high donor number and dielectric constant (49). Thus, strong chemical bondings are created between ether oxides and Li^+ (58). PEO also offers a high chain flexibility due to C-O-C backbones which increases the segmental mobility and so the ionic transport according to the VTF model. Finally, as mentioned by Golodnitsky and coworkers (67), PEO has a helical structure with six $O\text{-}CH_2\text{-}CH_2$ groups in two turns of the helix. PEO chains are wrapped around Li^+, that is why there could be an increase in ionic conductivity along the helix alignment as suggested by Armand (67). At 25°C, the reported best ionic conductivities for PEO:LiTFSI is around molar ratio O:Li = 10:1 and O:Li=8:1 (68). This is mainly due to the reduction of crystallinity rate and the increase in the number of charges carried. Long Chen *et al.* (69), showcased that from 60 wt% of salt, undissolved residual Li salt acts as a barrier for the Li^+ transport.

However, polymer-based PEO-LiTFSI electrolytes have residual issues that are limiting their use. Neat PEO exhibits a high crystallinity rate at room temperature (between 75% and 80%(70)) which limits its ionic conductivity to 10^{-6} $S.cm^{-1}$. Temperatures above the melting point of PEO (T_m=65°C), which means heating the battery, are mandatory to obtain a working system. Crystallinity rates change by a few percent with the molecular weight (36) and with the addition of Li salt. Thus, reported crystallinity values of PEO-LiTFSI are lower as shown by Hua Zhang and coworkers (68): 46% for PEO (M_n=600K):LiTFSI, O:Li = 12:1). Moreover, ether oxide groups create strong chemical bonding with Li^+. Trapped EO chains and coordinated cations with dipoles form stable complexes which increase the T_g and avoid fast cations migration (64). This phenomenon tends to limit the Li^+ conductivity at 25°C (49). In terms of PEO electrochemical stability, the reported voltage stability window is from 0.5V to 3.8V *vs.* Li/Li^+ (43). Such oxidation potential value makes impossible the use of high potential cathode active materials such as NMC with a working potential higher than 4V. Heng Zhang and coworkers (71) also warned about the low quality of the solid electrolyte interphase (SEI), formed at very low potential with alkali metals. Like other dual-ion conducting polymers, the transference number of PEO/LiTFSI is especially low (around 0.1)(64) which can induce cell polarization. Finally, the plasticizer effect of LiTFSI on PEO can make harder the processability, especially towards FFF 3D printing. In this case, a feeding too sticky and ductile due to the LiTFSI effect can lead to printing failure (24).

Even if PEO/LiTFSI electrolyte remains attractive, its limits lead to a maximal Li^+ conductivity of 10^{-6} $S.cm^{-1}$ at 25°C which is far below commercial electrolyte ionic conductivities (10^{-3} $S.cm^{-1}$). There is also a strong contradiction between electrochemical and mechanical performances toward 3D printing.

III. New strategies of PE

Many strategies have been imagined to overcome the low ionic conductivity at room temperature as well as limited electrochemical, thermal, and mechanical stability(72). That is why, the term Polymer Electrolyte (PE) hides several concepts of polymers-based systems from Solid Polymer Electrolyte (SPE) to Quasi Solid Polymer Electrolyte (QSPE) such as Gel Polymer Electrolyte (GPE). Different classifications have been early reported by Fiona Gray (73), Wright (74), Ratner (47), and coworkers until the 2000s. They have been mainly created based on different ways to improve ionic conduction through Li^+ motions mechanisms. More recently, other groups gave actualized classifications based on composition and morphologies (75)[Table 1.].

2023, (72)	**2022,** (51)	**2021,** (75)
Solid Polymer Electrolyte (SPE)	Amorphous macromolecular salt complexes	Architecturally Engineered Polymer matrix (AEP)
Composite Polymer Electrolytes (CPE)	Composite Polymer Electrolytes (CPE)	Solid Polymer Composite Electrolyte (SPCE)
Gel Polymer Electrolytes (GPE)	Gel Polymer Electrolytes (GPE)	
Polymeric Ionic Liquid Electrolytes (PILEs)	Polymer-in-salt or rubbery electrolyte	
	Plasticized system	

Table 1 Latest classifications of polymer electrolyte strategies

The classification of this work gives an overview of all strategies with main groups and subsets [fig.10]. Based on previous classifications, three classes can be identified: **Solid Polymer Electrolyte (SPE)** [line 1, Tab.1], **Composite Polymer Electrolyte (CPE)** [line 2, Tab.1], and **Quasi Solid Polymer Electrolyte (QSPE)** which gathers additional categories based on a poor mechanical behavior due to high loadings of plasticizer, ionic salt or ionic liquid**.**

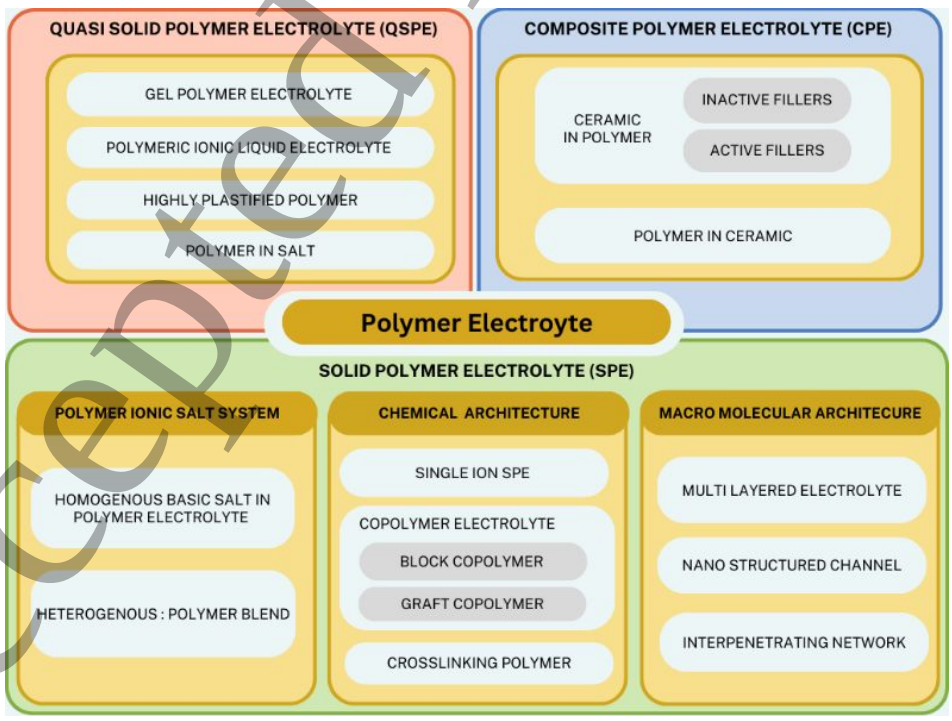

Figure 10 Polymer electrolytes classification

1. Quasi Solid Polymer Electrolyte (QSPE)

Gel Polymer Electrolytes (GPEs) are nonaqueous electrolyte solutions contained in a structural polymer matrix such as PVDF, PAN, or PMMA (51). These electrolytes could have a solid-like behavior if the liquid phase is entrapped in the polymer matrix. Li^+ motions mainly happen by diffusion in these entrapped regions(72). Thus, they reach liquid-like ionic conductivities (10^{-3} $S.cm^{-1}$) at room temperature with low volatility and low reactivity. However, GPEs suffer from poor mechanical behavior (poor rigidity and mechanical strength). It can cause damage by leakage of the liquid phase(72). Wookil Chae and coworkers (72) have compared ex-situ and in-situ methods of manufacturing for GPEs[fig.11]. According to them, in-situ polymerization by thermal initiator is the most efficient technique. They have reported high ionic conductivities up to $8.82x10^{-3}$ $S.cm^{-1}$ at room temperature for poly(vinyl formal)(PVFM)-based GPE (76). In terms of electrochemical properties, a GPE based on trihydroxymethylpropyl trimethylacrylate (TMPTMA) reaches an ionic conductivity of $6.15x10^{-3}$ $S.cm^{-1}$, a 0.1C discharge capacity of 183.1 $mAh.g^{-1}$ and 149$mAh.g^{-1}$ after 1 and 100 cycles respectively for an NMC811 *vs.* Li metal cell at 25°C (77).

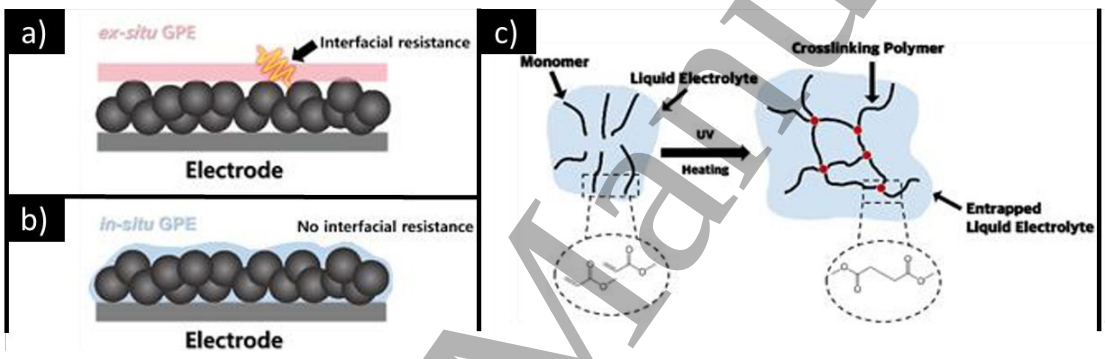

Figure 11 (a) Ex-situ polymerization (b) In-situ polymerization (c) In-situ polymerization UV or thermal activation. Adapted with permission from (72).

Polymeric Ionic liquid Electrolytes (PILEs) are made of polymer, ionic liquid (IL), and lithium salt. ILs are organic salts in which ions are poorly coordinated and melt below 100°C (78). They own high thermal stability, wide electrochemical windows, non-flammability properties, and low vapor pressure. They exhibit high ionic conductivity however, they do not have a solid-like behavior, so they suffer from poor mechanical stability (72,79). Thus, they have been polymerized to form polymers in which either the cation or the anion are incorporated into the polymer backbone (Polymerized ionic liquids (PILs)) (78). They have a solid-like behavior but the lower mobility of ions fixed to the polymer backbone results in lower ionic conductivity than ILs (80,81). It could explain why they are often used in electrolytes with IL and Li salt (81). Passerini and his group(82) have studied interactions between PILs, ILs, and Li salt. They have showcased that the addition of IL in PEO or PIL-based electrolytes can improve ionic conductivity up to $5x10^{-4}$ $S.cm^{-1}$ at 20°C. Higher ratios of IL/polymer are possible with PILs but it does not lead to higher conductivity and it makes electrolytes films sticker. Guo *et al.* (83) have reached an ionic conductivity of 10^{-3} $S.cm^{-1}$ thanks to their flexible ionogel electrolyte made of an immobilized ILs (1,2-dimethyl-3ethoxyethyl imidazolium bis(trifluoromethanesulfonyl)imide (DE-IM/TFSI)) into a hydrogen-bonded network of PIL copolymers bearing ureido-pyrimidinone (UPy) pendant groups(PIL-UPy). The quadruple hydrogen bonds and the electrostatic interactions between DE-IM/TFSI and PIL-UPy permit to obtain satisfactory mechanical strength with a high loading of DE-IM/TFSI (67.3 wt %).

Highly plasticized electrolytes are composed of polymer matrix, lithium salt, and a high content of plasticizers. The latter small molecules can enhance the polymer segmental motion and macro flexibility. Commonly, polar liquids, are added in polymer lithium salt systems. The result is a 100-fold increase in ionic conductivity. Lithium salt such as LiTFSI has also a plasticizer effect on the polymer matrix. PEO-based plasticized electrolytes reach ionic conductivity up to 10^{-4} S.cm^{-1} at 25°C (58). However, most plasticizers are very volatile that is why this solution is temporary, and high plasticizer loadings lead to the degradation of the electrolytes' mechanical behavior.

Polymer-in-salt electrolytes are composed of a small amount of high molecular mass polymers dissolved in low-temperature molten salt in large quantities (>50 wt%) (51). According to Hae-Kwon Yoon and coworkers (84), when salt is added above the critical concentration in these polymers, percolation of ions clusters provides fast cationic transport pathways (10^{-3} S.cm^{-1} at room temperature with 70 wt% of $LiCF_3SO_3$). Polymers must bring enough mechanical strength while having a high capacity to dissolve Li salt. to dissolve Li salt. Polyacrylonitriles (PAN) and polycarbonates are widely used. LiTFSI and LiFSI are often used as Li salt for their ability to be easily dissolved in polymers. However, PAN/LiTFSI-based electrolytes suffer from low backbones segmental mobility and polycarbonate-based systems suffer from deterioration of their mechanical behavior (85). For instance, graphene oxide filler in a PAN-LiTFSI polymer-in-salt system reaches an ionic conductivity of $1.1x10^{-4}$ S.cm^{-1} at 30°C (86). This kind of electrolyte still suffers from the low chemical and thermal stability of molten salt (85). Thus, hybrid solutions with polymer blends or inorganic fillers addition are developed to improve ionic conductivity and mechanical stability.

2. Solid Polymer Electrolyte (SPE):

Salt-in-polymer electrolytes are basic PE composed of a polymer matrix (>50 wt%) and Li salt. This type of electrolyte provides ease of process, flexibility, and good interfacial behavior with electrodes. However, limited conductivity together with a lack of rigidity and a low transference number (58) are the reasons why polymers with Li salt are just the starting point of other strategies to achieve efficient electrolytes. PEO/LiTFSI has been reported as the most efficient and studied couple but the PE exhibits a maximal ionic conductivity at 25°C around 10^{-6} S.cm^{-1}. Various couples of polymer/Li salt have been tested resulting in different properties (ionic conductivity, electrochemical and mechanical stability) (39,58). Indeed, Li salt does not have the same affinity and stability with polymers. Coordinating Li ions by carbonyl groups of polycarbonates and polyesters has been investigated as attractive alternatives to polyether (39). Aliphatic polycarbonate-based electrolytes can present improved ionic conductivity up to 10^{-5} S.cm^{-1} at 25°C and higher transference numbers due to weaker bonding between their polar group and cations (39). Polyester electrolytes also provide a higher transference number but showcase limited ionic conductivities on a wide range of temperatures with a maximum value of 10^{-6} S.cm^{-1} at 25°C and 10^{-4} S.cm^{-1} at 90°C (39). With an ionic conductivity of $2x10^{-4}$ S.cm^{-1} at 40°C, Michel Armand's group (87) has shown that a Jeffamine-based poly(ethylene-alt-maleic)/LiFSI electrolyte could outperform the ionic conductivity of PEO/LiTFSI. Besides, the cyclability at 70°C is improved thanks to the high amorphous rate of Jeffamine polymer.

Polymer blend electrolytes consist of a blend of two different polymers with complementary properties. The aim is to reduce the crystallinity of the ionic conductive polymer and bring enough mechanical strength to improve electrolyte mechanical properties. In the case of miscible polymers, the electrolyte is composed of one phase and both polymers can be involved in ionic transport. Ragones *et al.* (38) have 3D printed an electrolyte based on the miscible blending of PEO and PLA. The overall crystallinity corresponds to the one of PLA which is the lowest and the overall ionic conductivity of such a blend is lower than a classical PEO/LiTFSI. According to the authors, this is due to a non-optimized printing procedure leading to an incomplete mixability of these two polymers. Some Li^+

could also interact with PLA which has not the same ability to convey Li^+, especially at low temperatures due to the high glass transition temperature of PLA (60°C). Dolle and coworkers obtained the same conclusion with a blend of PVP (T_g=100°C) and PEO. They have also studied immiscible polymer blend electrolytes processed by extrusion(49). In this case, one phase can be responsible for ionic conductivity and the other can act as a mechanical reinforcement phase. Reported PEO-based polymer blends have an ionic conductivity in a range of 10^{-6} to 10^{-4} S.cm^{-1} at low temperatures (58).

Single-ion polymer electrolytes (SIPEs) are able to conduct only one type of ions thanks to covalently bonded anions to their chain or anion acceptor sites to immobilize anions (88) [fig. 12(a)]. It results in a Li^+ transference number close to the unity against t_+=0.1 for PEO/LiTFSI electrolyte (64). Thus, it permits to reduce cell polarization upon cycling, to limit the decomposition of the electrolyte and Li dendrite nucleation (75,88) [fig. 12(b)]. However, SIPEs usually present ionic conductivities lower than 10^{-4} S.cm^{-1} at room temperature because of anions immobilization(88), higher T_g(88), and strong ionic interactions with Li^+(75). Their poor cycling stability and difficult synthesis process might be also problematic for large-scale applications (51). Recent studies succeeded in reaching higher conductivity up to 10^{-3} S.cm^{-1} by adopting novel strategies. Thanks to a semi-interpenetrating network of PMMA/lithium polystyrene sulfonate (LiPSS)(89), the high transference number of 0.91 demonstrates the ability to inhibit lithium dendrite growth [fig. 12(c)]. Another strategy is to immobilize anions in the molecular structure by playing with anion size(72). Zeyu Li and coworkers have synthesized poly(lithium 4-styrene sulfonate)-carbon quantum dots (PLSSCQD) particles and blended them with PEO. The big size of CQD anions and hydrogen bonding immobilized them in the polymer matrix. [fig. 13 (d)] They depict a room temperature ionic conductivity of 2.20x10^{-4} S.cm^{-1}.(90)

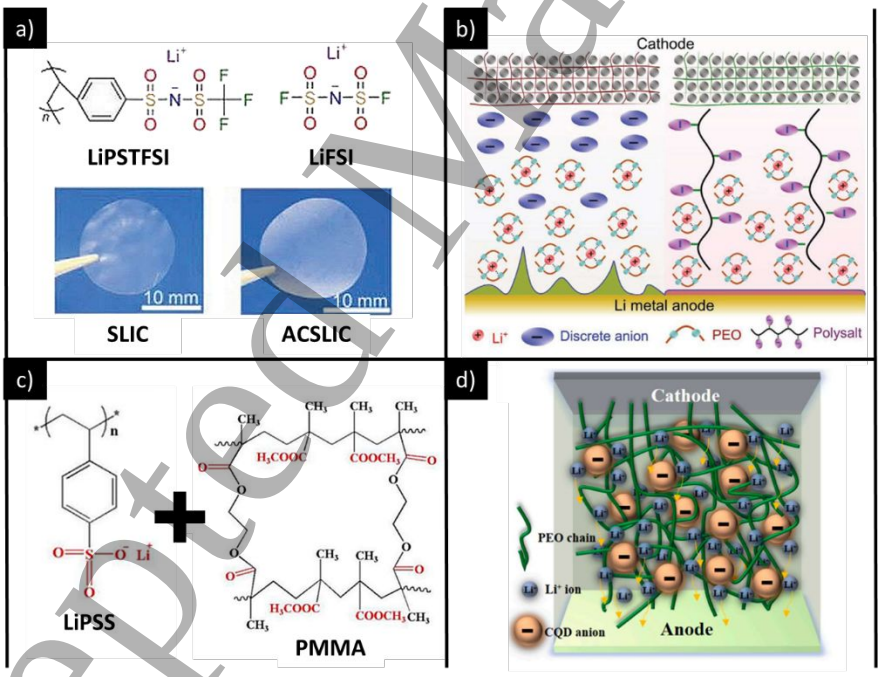

Figure 12 (a) Chemical structures of lithium poly[(4-styrenesulfonyl)(trifluoromethanesulfonyl)imide] (LiPSTFSI) and lithium bis(fluorosulfonyl)imide [Li[N(SO2F)2] (LiFSI), and corresponding electrolytes membranes (Single Ion Conductor (SLIC) and Additive Containing SLIC (ACSLIC))reproduced from (88) © 2019 with permission from Elsevier (b) Positive effect of Single Ion conductor against dendrite growth in LMB reproduced from (88) © 2019 with permission from Elsevier (c) Lithium polystyrene sulfonate + poly(methyl methacrylate) electrolyte, reproduced from (89) © 2021 with permission from Elsevier (d) CDQ anions blocked in PEO matrix (90)

Copolymer electrolytes contain a homopolymer in which another monomer unit is introduced to offer different properties (stiffness(91), segmental mobility(92), crystallization(93)). This latter can be grafted on a main backbone, randomly or alternatively introduced to the main polymer backbones, or

organized in block copolymers (75). Grafted and block copolymers have been the two main studied families so far. Polymers with EO units, such as PEO, are the most attractive conductive parts while PS is widely used for mechanical reinforcement. This strategy can enhance ionic conductivity at 25°C thanks to crystalline modifications and strengthening of the mechanical behavior. According to Devaux *et al.* (92) linear PS-PEO-PS, is a good compromise between mechanical behavior and ionic conductivity. They showcased that 30 wt% of PS is necessary to obtain percolation of PS and thus self-standing films which exhibit an ionic conductivity of $1x10^{-4}$ $S.cm^{-1}$ at 60°C. Even if they hinder recrystallization at low temperatures, comb PEO block-copolymers suffer from poor capacity retention(92). Bouchet and coworkers (65) have highlighted a "dead zone" effect at interfaces between conductive and mechanical blocks. This region is characterized by an absence of conduction and crystallization due to low segmental mobility. A decrease in the proportion represented by these excluded zones can be achieved by increasing the PEO molar weight. It should be noted that, at temperatures above the melting point where crystalline regions disappear, block polymer electrolytes showcase lower ionic conductivities (lower fraction of PEO domains) and higher mechanical strength due to their mechanical parts. That is why ionic conductivity improvement compared to PEO homopolymer electrolytes happens below the PEO melting point (around 40°C) (65). Armand and coworkers (91) have worked on Jeffamine-PS copolymer. They obtained well-balanced electrolyte properties with $7.9x10^{-5}$ $S.cm^{-1}$ at 40°C with improved cycling capability due to a stronger mechanical behavior. They have highlighted a drop of conductivity with a PS side moieties content increase which can be related to a lower fraction of conducting volume and a higher tortuosity. Copolymer electrolytes can also be made by in situ synthesis. A comb-like copolymer PLA/PEG with LiTFSI was in-situ photopolymerized by UV light to achieve a polymer electrolyte with an ionic conductivity of $6.9x10^{-5}$ $S.cm^{-1}$ at 25°C.(94)

Crosslinking polymer electrolytes consist in linking one polymer chain to another one through covalent bonding. Similarly, to polymer blending strategy, it improves the tensile strength and hinders crystalline domains in polymers. However, it permits to obtain more stable morphologies. Most of the crosslinked polymer electrolytes are made through the thermal decomposition of a crosslinking agent or irradiation by UV light. However, crosslinking of polymers can have a negative effect on the conductivity as it can restrict polymer chains' mobility (56). It could explain why reported ionic conductivities are in the range of 10^{-6}-10^{-5} $S.cm^{-1}$ (95). The crosslinking between PEO and a polymer with a lower Li salt dissociation ability results in a loss of O-Li^+ interactions so a higher transference number. This is the case of the crosslinked electrolytes of PEO and poly(tetrahydrofuran) (PTHF) realized by Mackanic and coworkers (95). Porcarelli *et al.* (96) have reached a higher ionic conductivity of 10^{-4} $S.cm^{-1}$ at room temperature by in-situ UV photopolymerization technique. They have successfully crosslinked PEO and tetraglyme (TEGDME) thanks to a photoinitiator.

Inter-Penetrating Networks (IPN) electrolytes are composed of two or more distinct crosslinked polymer networks with no covalent bonds between them. Compared to crosslinked electrolytes, the mechanical stability between the two immiscible phases is only ensured by the interpenetrating character of the structure. They are usually obtained by sequential or simultaneous polymerization. Semi-IPNs are composed of one or several polymer matrixes penetrated by linear or branched polymer at the molecular scale (75).

Multilayered polymer electrolytes are composed of different layers to mechanically and chemically adapt interfaces with each electrode. This strategy is used to avoid side reactions of the electrolyte with electrodes which can be restrictive in other strategies. Xavier Judez and coworkers (97) have developed a bilayer electrolyte composed of PEO/LiFSI + Al_2O_3 at the Li metal side and PEO/LiFSI + Lithium Ion Conducting Glass-Ceramic (LICGC) at the cathode side. This divided electrolyte structure

hinders LICGC reactions with Li metal. This strategy is interesting for high-potential battery applications but provides more solid/solid interfaces which increase the overall impedance of the cell. It also makes harder the processability of the cell.

Nanostructured electrolytes are made of specifically structured channels to improve ionic conductivity by providing fast Li^+ motion pathways. The goal is to control the morphology of the electrolyte to create nanoscale channels to avoid the tortuosity of pathways and to ensure a direct, fast ionic transport. This strategy is used for composite electrolytes where ceramics 3D networks can be obtained by sintering and impregnation or by electrospinning of ceramics nanofibers. Fu *et al.* (98) have made the most ionic conductive garnet additive by creating ceramics fibers thanks to electrospinning. Yu and coworkers (99), have used nanostructured hydrogel to manufacture their 3D garnet framework to reach ionic conductivity of $8.5x10^{-5}$ $S.cm^{-1}$ at ambient temperature. Kihun Jeong *et al.* (100) have created a single ion conducting covalent organic framework (COF) by a solvent-free method. Their nano conductive channels, with a diameter of 11.8 Å, permit to enhance the ionic conductivity to $2.7x10^{-5}$ $S.cm^{-1}$ and to obtain a $t_+ = 0.9$ at room temperature.

4. Composite Polymer Electrolyte (CPE)

Composite polymer electrolytes (CPE) are made of a polymer/Li salt matrix loaded by inorganic fillers. Added particles can present electrochemical and mechanical performances whereas organic phases can catch their poor processability and interfacial properties up. Since the first reported work in 1982, several studies have been produced toward a better understanding of CPE behaviors (52,101,102).

There are two types of particles: **active fillers** can conduct Li^+ in their structure(103) contrary to **passive fillers**. In both cases, Li^+ transport can happen **in the matrix** or at the **interface polymer-ceramic**. In the polymer matrix, ionic motion mainly occurs in the amorphous phase according to previously described mechanisms. Ionic conductivity in the polymer or at the interface polymer-ceramic is mainly improved by chemical and mechanical interactions between inorganic filler and polymer matrix. In the case of active fillers, there are two more possibilities for Li^+ conduction: **ceramic pathway** and **hybrid pathways** (polymer + ceramic) [fig.13]. (102)

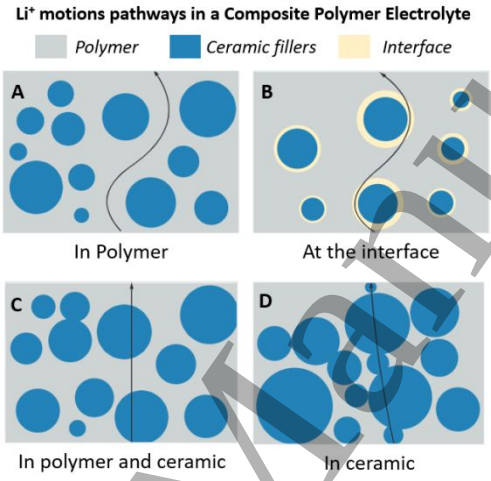

Figure 13 Li^+ conduction pathways in a composite polymer electrolyte in (a) Polymer, (b) Interface, (c) Polymer and ceramic, (d) Ceramic adapted from (102) © 2020 with permission from Elsevier

Various key parameters have been identified to manufacture CPE:

- **Type of fillers:** passive or active fillers do not enable the same Li^+ motion pathways (102).
- **Surface chemistry**: Lewis acid-base interactions with lithium salt facilitate salt dissociation and thus avoid ion clusters(104) and immobilize anions (105). Fillers' surfaces also interact with the polymer matrix (act as a solid plasticizer) (101). Filler surface modification could be an efficient strategy to achieve an ionic conduction pathway at the interface and reduce the fillers/polymer interfacial resistance (80,102).
- **Size:** nanopowder fillers mean a higher specific area hence providing more interactions with the polymer matrix(106) (decrease in crystallinity, rise in free Li^+ fraction, widen the electrochemical stability window) (106). Fillers granulometry also influences the optimal loading which gives the best conductivity (107).
- **Shape:** 0D (particles) is the most used shape of particles but it is limited by agglomeration issues. 1D fillers (nanowire, nanofiber) provide a more continuous path than spherical ones. It is a convenient strategy for active fillers to avoid polymer/ceramic interfaces so as to offer a continuous pathway for Li^+ in ceramics (104). 2D nanosheets/flakes can create larger active interfaces. A 3D framework of active fillers directly conveys Li^+. They are usually realized by porous network impregnation or electrospinning techniques of 3D fiber networks (108).
- **Concentration:** At low loadings (<10 vol%), enhancement of ionic conductivity is linked to a drop of crystallinity, an improved Li^+ dissociation, and an increase of filler/polymer interfaces

(79,109). There is an optimal content of fillers which gives a maximal ionic conductivity. Below this threshold, ionic conductivity is limited because of lower interactions with the matrix and a higher crystallinity rate. Above this loading, percolation can happen meanwhile rising the risk of agglomeration, thus raising the tortuosity of Li^+ pathways in the polymer. Processability is also becoming difficult with an increase in hardness and brittleness (110). Based on this assumption, the difference can be made between:

  - *Ceramics-in-polymer* which are low-loaded electrolytes in which the ionic conductivity is improved, processability is easy but transference number and stiffness remain low.
  - *Polymer-in-ceramic* which are high-loaded electrolytes in which stiffness and transference number are high but the ionic motion can happen through ceramic particles only if the interfacial resistance between organic and inorganic phases is decreased (69). They are considered as promising solid electrolytes because they can gather advantages from both inorganic and organic solid electrolytes (111). These electrolytes are more suitable for large batteries because of their better mechanical behavior which makes them safer than ceramic-in-polymer systems (69).

- **Manufacturing methods:** The manufacturing process has also a key role to play to obtain a homogeneous dispersion of fillers and enable the construction of continuous and uniform transport channels for Li-ion migration (79). Mechanical dispersion of fillers inside a matrix is the easiest way but particle agglomeration is hard to hinder. Chemically organized fillers (grafted particles, in-situ synthesis(112)) permit to reduce efficient interfacial resistance between particles and polymers. Finally, mechanically organized fillers (Interpenetrating networks, fillers positioning thanks to rheological behavior, 3D ceramics networks backfilled with a polymer electrolyte) create continuous ceramic pathways in the case of active fillers.

A. Passive fillers

SiO_2, Al_2O_3, TiO_2, and ZrO_2 have been mainly used as passive fillers to enhance ionic conductivity [fig 15.]:

- *In the polymer:* The aim is to reduce the crystallinity of the host matrix by mechanical wrapping around fillers and chemical bonding with polymer chains [fig. 14]. Mechanically, inert nanoparticles contribute to increase segmental motion by increasing the free volume (52). Chemically, Lewis acid groups on the surface of fillers can compete with Li^+ to complex with oxygens of PEO and hinder its recrystallization (104). Thus it generates a drop in the polymer's crystallization rate and glass transition temperature (T_g) (113).
- *At the interface:* Reported works also highlighted an ionic conductivity enhancement at high temperatures when the polymer is already in an amorphous state. They demonstrated that specific interactions happen between fillers and the matrix. Indeed, Lewis acid groups on the surface of particles can compete with Li^+ to complex counter anions and help to dissociate Li salt and avoid ion clusters. It promotes ionic transport by creating fast pathways at interfaces (113) (114)[fig. 15]. It also increases the Li^+ transference number (101) and the number of free Li^+ (104).

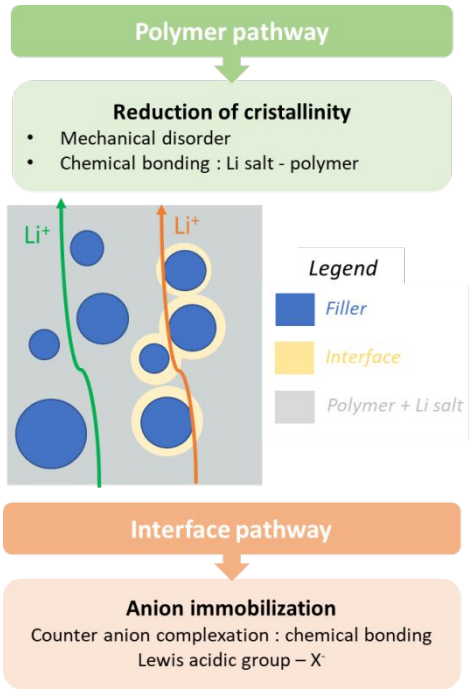

Figure 14 Li^+ pathways in CPE with passive fillers

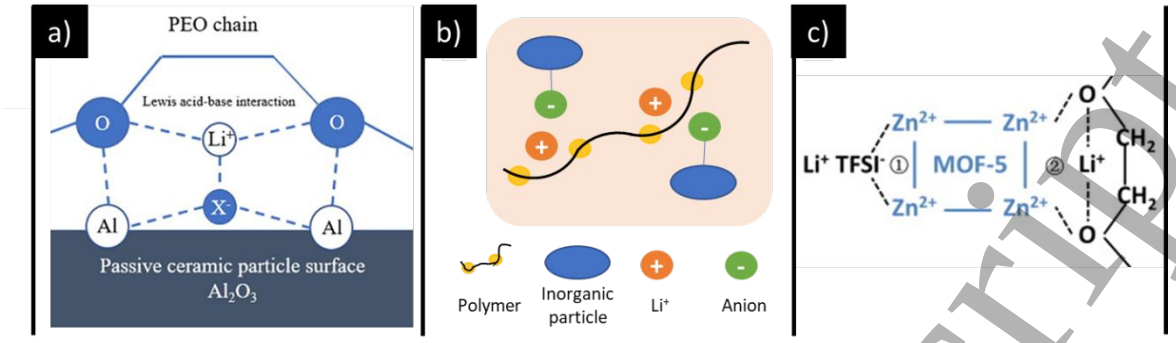

Figure 15 Chemical interactions at the interface nanosized inorganic fillers and polymer/salt matrix (a) PEO-LiTFSI/ Al_2O_3, adapted with permission from (104), (b) Immobilization of anions through interactions with nanosized inorganic particles (c) PEO-LiTFSI/ MOF-5, adapted with permission from (114) © 2013 with permission from Elsevier

Croce and coworkers (64) studied the enhancement of transport properties of PEO-LiX systems with **nanoparticles of TiO_2 or Al_2O_3** inside. Differences in performances for 3 PEO-$LiSO_3CF_3$-Al_2O_3 systems at temperatures above the PEO melting point illustrate a promoting effect of specific interactions between ceramic surface and PEO chain/Li salt (via hydrogen bonding). That is why high acidity fillers such as TiO_2 are suitable for increasing the conductivity. It increases the free Li^+ ions amount which can move faster throughout the conducting pathways at the ceramic extended surface. The transference number also rises up to 30% (106). TiO_2 (1 wt%) doped PEC-LiFSI reaches a t_+ of 0.8 with an ionic conductivity of $1.4x10^{-4}$ $S.cm^{-1}$ at 40°C (64). S. Das and A. Ghosh (115) have also worked on PEO-LiTFSI-Al_2O_3 systems. Addition from 0 to 20 wt% of Al_2O_3 in a PEO (Mw 400K) LiTFSI (O:Li = 12:1) electrolyte reveals a minimum of PEO crystallinity of 14 % with 5 wt% of Al_2O_3, which corresponds to a maximal ionic conductivity. However, the decrease in crystallinity is not significant (18% of crystallinity without fillers) so the main chain dynamic of the host polymer matrix does not change significantly. Dispersed SiO_2 can improve ion-conduction behavior up to a loading of 10 wt% of because of agglomeration issues (52). A chemically organized dispersion of particles could create Li^+ conduction pathways at the interface ceramic/polymer as well as reduce more drastically the polymer crystallinity. **Modified SiO_2 nanoparticles** have been widely studied to promote Li salt dissociation and avoid filler agglomeration such as Porous Vinyl Functionalized (PVF)-SiO_2,(116), or walnut-like SiO_2,(117). A deeper investigation of SiO_2 inert fillers/Li salt interactions demonstrated that the functionalized silica surface plays a major role in LiTFSI dissociation. SiO_2-Li particles induce a drop of one decade in terms of conductivity (105). A threshold of conduction exists at a sufficient amount of fillers inside the matrix. Snehashis Choudhury *et al.* (118) have used hairy nanoparticles of SiO_2 grafted with hydroxyl end-chain groups of PEO. These nanoparticles were then crosslinked with PPO to bring the mechanical resistance. Such a technique enables to reach high mechanical modulus of the membrane which still needs to be soaked with liquid electrolyte to achieve high ionic conductivity. **In-situ synthesis of particles** in the polymer matrix is another way to reach this goal. Dingchang *et al.* (119) have showcased that in-situ synthesis of SiO_2 nanospheres in a PEO (M_V=600K) matrix can reduce polymer crystallinity rate by chemical bonding and mechanical wrapping. Xu and coworkers (110) succeeded in dispersing homogeneously SiO_2 particles by in situ synthesis in a PEO network. The low PEO crystallinity leads to a conductivity of $1.1x10^{-4}$ $S.cm^{-1}$ at 40°C. In their exhaustive review, Zheng and coworkers (52) have reported ionic conductivities from 10^{-6} $S.cm^{-1}$ to 10^{-4} $S.cm^{-1}$ for passive particles dispersion in a polymer matrix.

B. Active fillers

Perovskite (LLTO), NASICON (LAGP), sulfide (LGPS) and garnet (LLZO) have been mainly used as active fillers (75). Perovskite-structured fillers provide lower ionic conductivity compared to the other fillers and can be reduced at low potential (*vs.* Li/Li^+) (80). NASICON-type fillers are good candidates to reach liquid-like ionic conductivity up to 10^{-2} $S.cm^{-1}$ at room temperature but their rigid nature induces interface issues with electrodes and Ti-containing particles are not stable at low potential (120). This is also the case with sulfide additives. Garnet-type particles show ionic conductivity up to $1x10^{-3}$ $S.cm^{-1}$ at room temperature with a wide electrochemical stability domain. Acidic groups on these particles bind to the salt anions which furnishes the shared electron pair as Lewis base (121). It immobilizes anions and therefore increases the transference number. In their extensive review of garnet-type solid-state fast Li-ion conductors, Thangadurai and coworkers(122) reported the highest ionic conductivity at 25°C, $1x10^{-3}$ $S.cm^{-1}$, for LLZTO ($Li_{6.4}La_3Zr_{1.4}Ta_{0.6}O_{12}$), thanks to its pure cubic garnet structure (123). Zr- and Ta-based materials are stable on a wide potential range (up to 6V *vs.* Li/Li^+ at 25°C) and appear stable against chemical reactions with Li metal (124). That is why the following section mainly emphasizes PEO/Ta-doped LLZO CPE in which ionic conductivity can be enhanced:

- *In the polymer:* in the same way as passive fillers interact, it hinders the polymer crystallization.
- *At the interface:* space charge region enhances the ionic conductivity. Free energy difference leads to Li^+ migration at the surface of fillers, which leaves negatively charged vacancies in the lattice(101).
- *In the fillers:* Li^+ movement follows the Arrhenius model inside particles. Li cation can also move in both, polymer and fillers, through a hybrid pathway [fig. 16]. However, the high interfacial resistance between particles and polymers makes this kind of pathway impossible(102).

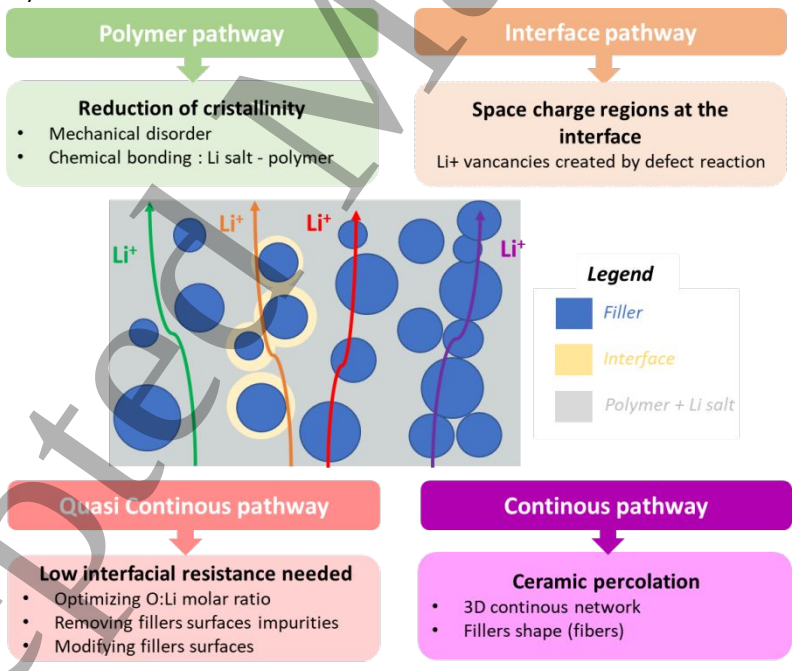

Figure 16 Main mechanisms for Li^+ motion in CPE with active fillers

Dispersion at low loadings: Ionic conductivity increases with the content of fillers up to a **maximum of around 10 and 15 wt%,** which depends on the powder granulometry (98,111). Hua Zhang and coworkers (68) have shown that crystallinity can be divided by 2 thanks to the addition of LLZTO nanoparticles in a PEO/LiTFSI matrix. This increase in ionic conductivity below the LLZTO percolation threshold shows that dispersed nanofillers can improve the ionic conductivity in the polymer matrix (more free volume for PEO chains motions, and decrease of the crystallinity) (69). However, better

ionic conductivity values have been obtained for a PEO:LiTFSI (EO:Li = 8:1 to 12:1) with 10 wt% of LLZTO nanoparticles, than for a classical PEO-LiTFSI system and PEO-LiTFSI with SiO_2 or ZrO_2 (52). Interactions between PEO, LLZTO particles, and Li salt create Li vacancies at the LLZTO surface, sites for ionic conduction at the interface (120). Around 10 wt% of LLZTO also leads **to better cycling stability** compared to PEO-LiTFSI due to dendrite suppression and better stability at the anode interface. Indeed, it tends to reduce the PEO area exposed to Li metal and reduce the formation of a passivation layer of Li_2O. Interfacial effects at the polymer/garnet interface are usually displayed to explain enhanced ionic conductivities. Jingxian Zhang *et al.* (107) have studied Li salt-free electrolyte PEO/LLZTO to avoid the segmental motion effect and just analyze the effect of the PEO/LLZTO interaction. Their electrolyte provides an ionic conductivity of $2.1x10^{-4}$ $S.cm^{-1}$ at 30°C for 12.7 vol% of LLZTO nanopowder due to the space charge region at the interface. Jin Zheng *et al.* (125) have found that EO:Li molar ratio has a critical role to play in conductive interface formation. According to them, LGPS particles are softer than LLZO that could explain a less challenging interface formation in their LGPS-PEO (70 wt% EO:Li = 9:1) electrolyte which exhibits an ionic conductivity of $2.2x10^{-4}$ $S.cm^{-1}$ at 25°C.

Dispersion at high loadings: It can create new Li^+ motion pathways through fillers if the strong **interfacial resistance of ceramics/polymer** is overcome. In the case of dispersed nanoparticles, this resistance hinders hybrid pathways and Li^+ motion only happens in the organic phase. It explains that higher loadings induce lower ionic conductivity by decreasing the percolating amount of polymer and increasing the tortuosity of conducting pathways. Moreover, higher loading of fillers leads to aggregation due to a surface energy gap between fillers and polymer (126). Jing Zheng and Yan-Ya Hu (127) have showcased this phenomenon by studying PEO/LiTFSI electrolytes with LLZO from 5 to 50 wt%. At 20 wt%, no improvement is observed due to the blocking effect of particles. At 50 wt%, the percolation threshold is overtaken and LLZO is the main source of Li^+ which can be carried. However, there is no significant enhancement of ionic conductivity because of grain boundary interfacial resistance and particle blocking effect (127). It is also the origin of the lower ionic conductivity ($1.12x10^{-5}$ $S.cm^{-1}$ at 25°C) obtained by Chen-Zi Zhao *et al.* (121), with their electrolyte composed of 40 wt% of LLZTO particles in PEO/LiTFSI matrix. Despite this, their electrolyte provided a wide electrochemical window (up to 5.5V *vs.* Li/Li^+) and a t_+ of 0.58 at 25°C. Gupta and Sakamoto investigated interfacial resistance origins (128). A layer of impurities (Li_2CO_3) on LLZTO nanoparticles resulting from proton exchange when the sample is exposed to moisture creates a barrier to Li^+ and is responsible for electrostatic repulsion with PEO. With an appropriate **heat treatment** of LLZTO (700°C for 10h under argon) and a convenient amount of LiTFSI (EO:Li = 15:1), they succeeded in sharply decreasing the interfacial resistance [fig. 17(a)]. Eveline Kuhnert *et al.* (102) have also tried to lower interfacial resistance in a PEO/LLZTO electrolyte. They have **grafted PEO backbones on LLZTO** thanks to CTMS (3-chloropropyl) trimethoxysilane. They have been able to reduce the interfacial resistance and enable higher Li^+ conductivity through the interface [fig. 17(b)]. CTMS has been also involved in the chemical bonding of LGPS microparticles with PEO backbones which results in an ionic conductivity of $9.83x10^{-4}$ S/cm at 25°C with a high Li^+ transference number of 0.68 (against $2.42x10^{-4}$ S/cm and 0.58 for a dispersed LGPS in PEO) (129) [fig. 17(c)]. Li^+ motion has been greatly enhanced thanks to LGPS bulk properties, weaker Li-sulfide interactions than Li-oxygen, and a reduced grain boundary resistance between particles. Authors have also blended PEO with 2 widely different molecular weights (2,000 and $1x10^6$) to facilitate the bonding with CTMS and provide faster Li^+ pathways through the vehicular mechanism. Zeya Huang *et al.* (130) have also demonstrated that modifying interfaces in the organic-inorganic composite electrolyte is an efficient way to improve ionic conductivity, thermal stability, and electrochemical performances. Their polydopamine coating on LLZTO nanoparticles (80 wt %) allows to reduce strongly the interfacial resistance (4 times lower at 50°C) with PEO/LiTFSI (20 wt%) which

results in a promising ionic conductivity of $1.15x10^{-4}$ S.cm^{-1} at 30°C. This enhancement effect is mostly due to a more homogenous particles distribution and facile Li^+ pathways created at the interface. At these loadings, LLZTO-loaded PEO-LiTFSI electrolytes present better performances than ZrO_2-loaded ones.

Mechanically, high loadings of fillers permit to reach sufficient mechanical resistance to prevent lithium dendrite growth (131). For instance, Li *et al*. (111) have extruded a PEO-LiTFSI electrolyte with 75 wt% of LLTO, which exhibits a high tensile strength (3.85 MPa) preventing the formation of dendrites. Long Chen and coworkers (69) have also studied the effect of adding LLZTO microparticles from 0 to 80 wt% in a PEO-LiTFSI (O:Li = 8:1) electrolyte. At 80 wt%, the addition of a plasticizer such as PEG is necessary to have enough flexibility to keep mechanical integrity. Ionic conductivities remain lower for polymer-in-ceramic (80 wt%) than for ceramic-in-polymer (10 wt%) systems.

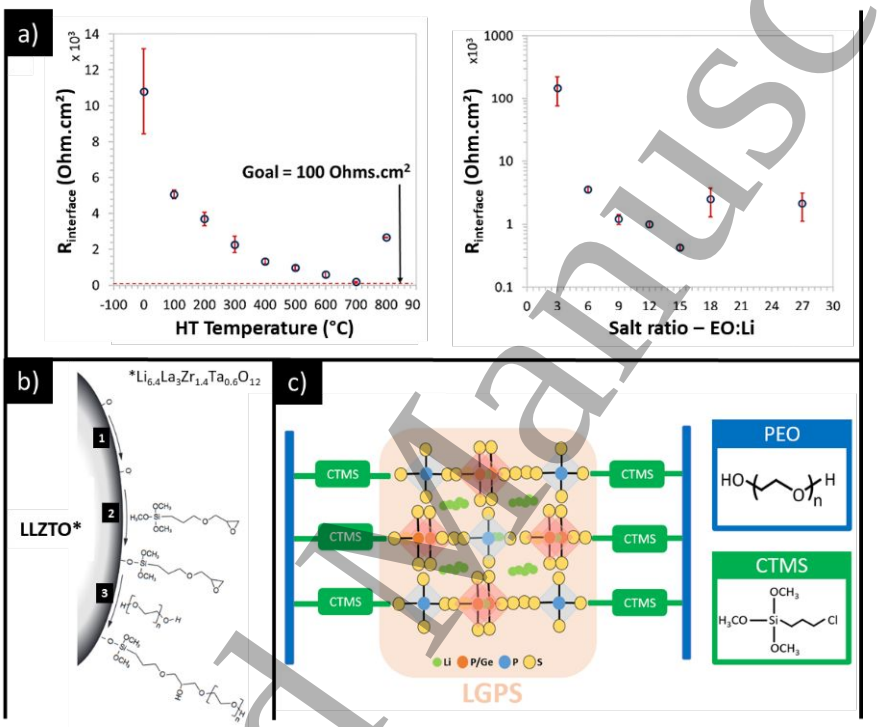

Figure 17 (a) Optimal EO:Li and heat treatment to reduce LLZTO/PEO interface, adapted with permission from (128) © 2020 with permission from Elsevier, (b) PEO grafting on CTMS-coated LLZTO, adapted with permission from (102) © 2020 with permission from Elsevier, (c) LGPS linked to PEO through CTMS

3D continuous ceramic pathways: In order to overcome interfacial resistance and take benefit of the ionic transport performances of ceramics, researchers attempted to create 3D continuous Li^+ pathways. MJ. Palmer *et al.* (109) have created a high-loaded electrolyte made of a 3D framework of conductive ceramics (77 wt%). They sintered a thin layer of LATP microparticles and then backfilled it with a crosslinked polymer electrolyte based on PEO/Jeffamine and LiTFSI to manufacture a 25µm thick composite electrolyte [fig. 18(a)]. They obtained an ionic conductivity two orders of magnitude greater than that of a dispersed ceramic system ($3.5x10^{-5}$ S.cm^{-1} at 20°C). Electrospinning is another method widely used to generate high-loaded ceramic-polymer nanofibers. These nanofibers form a 3D ultra-conductive network which can be backfilled by a polymer electrolyte. Mengmeng Zhang *et al.* (132) have reached an ionic conductivity of $1.05x10^{-4}$ S.cm^{-1} at 50°C thanks to their LLZTO/PVDF/PEO network in a PEO/LiTFSI matrix. A slightly higher conductivity of $2.15x10^{-4}$ at 25°C has been obtained for a similar method with PVP/LLZTO fibers (98)[fig. 18(b)].

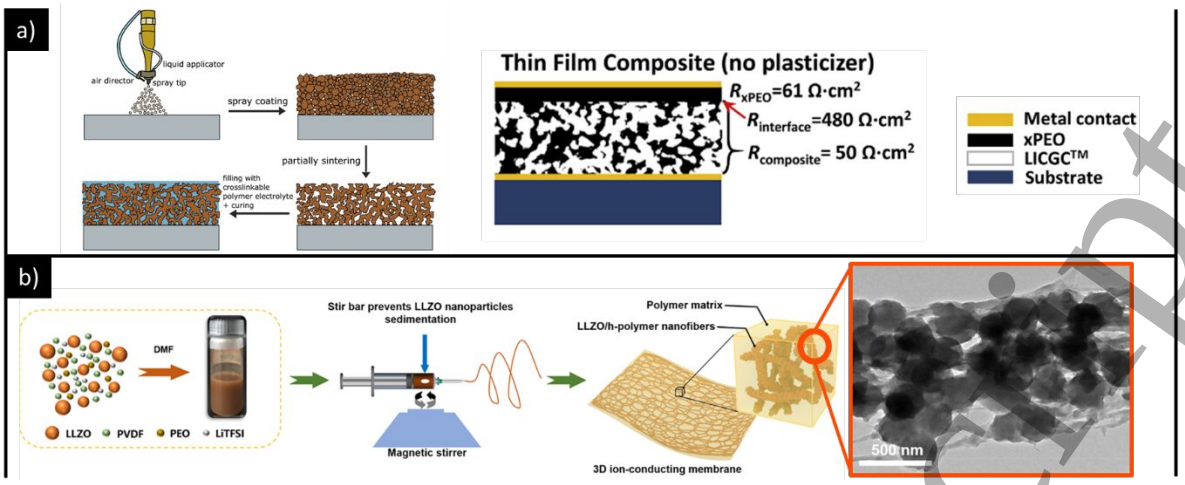

Figure 18 3D ceramic network strategies to create continuous ceramic pathways : (a) Sintered 3D network of LICGC, post-filled by PEO, adapted with permission from (109) © 2020 with permission from Elsevier, (b) Electrospinning of PEO-LLZO fibers, adapted with permission from (132) © 2021 American chemical society

Thus, main advantages of these different strategies can be classified regarding their: mechanical stability, ionic conductivity, transference number, and electrochemical stability [fig. 19]. Compatibility of these strategies with FFF printing specifications is discussed below to identify the method which can provide the highest ionic conductivity at room temperature with an electrochemical stability window compatible with an LFP/graphite cell cycling.

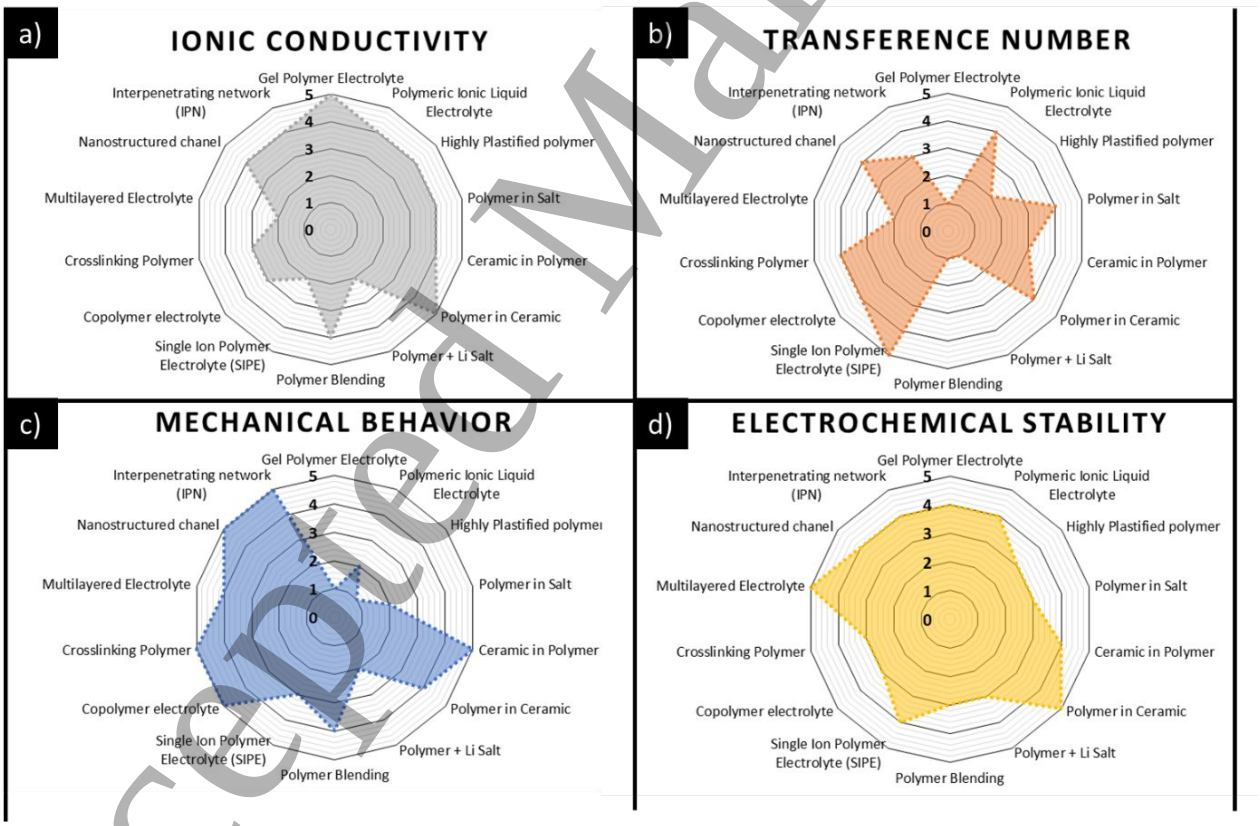

Figure 19 Radar diagrams of polymer electrolyte strategies in terms of ionic conductivity, transference number, and mechanical and electrochemical stability at room temperature. Each characteristic is graded from 0 to 5: (a) Ionic conductivity ≤ 10^{-8} S.cm^{-1} [level 0] and ≥ 1x10^{-3}S.cm^{-1} [level 5] ; (b) Transference number ≤ 0.1 [level 0] and ≥ 0.9 [level 5] ; (c) Mechanical behavior liquid behavior [level 0] and stiffness, self-standing film [level 5] ; (d) electrochemical stability unstable [level 0] and stable from 0 to 4.5V [level 5]

III. In-space 3D printing of PE by FFF

1. FFF printing specifications

Based on this landscape of strategies, the aim is to identify potential approaches for 3D printing a polymer electrolyte by FFF 3D printing. In this process, two counter-rotative rolls carry a polymer-based filament in a heating block through a PTFE duct. Polymer melts in the heating block and filament acts as a piston driving melted materials out of the printing head through the nozzle(133). Obviously, filaments have to contain a minimal amount of thermoplastic polymer which restricts the quantity of fillers in the case of loaded filaments. Despite the great versatility of this process, specific mechanical and rheological behaviors are needed to qualify a filament as "FFF printable". Thermal properties are also important to ensure good adhesion between each printed layer. All of these requirements can strongly go against ionic conductivity properties of electrolytes.

Mechanical properties of the filament will influence the feedability. The filament must have a **low ductility** not to be crushed by feeding rolls. If it is not the case, it will pass through feeding rolls with a high contact area that induces winding of the filament around rotating rolls (134). Go *et al.* (135) have showcased that it occurs when the extrusion force is higher than a critical force linked to the shear strength of the material and lower than the needed force to push melted material in the heating block [fig. 20(a)]. However, a too-low ductility filament can be very brittle and break in the print head (130) [fig. 20(b)]. In the case of composite feedstock, this brittleness increases significantly with the loading of fillers. (136) The filament must also **have enough stiffness** to avoid buckling after feeding rolls (137). It is acting as a piston which has to apply a minimal pressure on the melted material to exit it from the nozzle. According to Venkatarman *et al.* (133), this needed pressure is proportional to the melt viscosity. Thus, they have used the ratio of Young modulus on melt viscosity to predict filament buckling [fig. 21(a)]. Arrigo and Frache (137) have applied this model to the 3D printing of different commercial PLA filaments. With their parameters (nozzle 0.4mm, print speed 30mm.s^{-1}), the critical ratio was around 4x10^{-5} s^{-1}. **A minimal flexibility** is also important to obtain a spoolable filament and to avoid filament rupture. Finally, a **too-sticky** filament can adhere to the rotating roll or the PTFE sheath of the heating block. It results in winding or blockage of melted material in the PTFE sheath. Thus, Maurel *et al.* (24) have tried to adapt the printer by suppressing the PTFE tube to 3D print a PEO: LiTFSI (O:Li = 20:1) system. Studies have been devoted to quantifying the required mechanical properties for the feedability of an FFF 3D printer. Through 3-points bend tests, buckling tests, and hardness tests, mechanical properties have been confronted with the printability. A correlation has been demonstrated between filament hardness and printability (138) [fig.20(c)]. These features are coupled with rheological behavior.

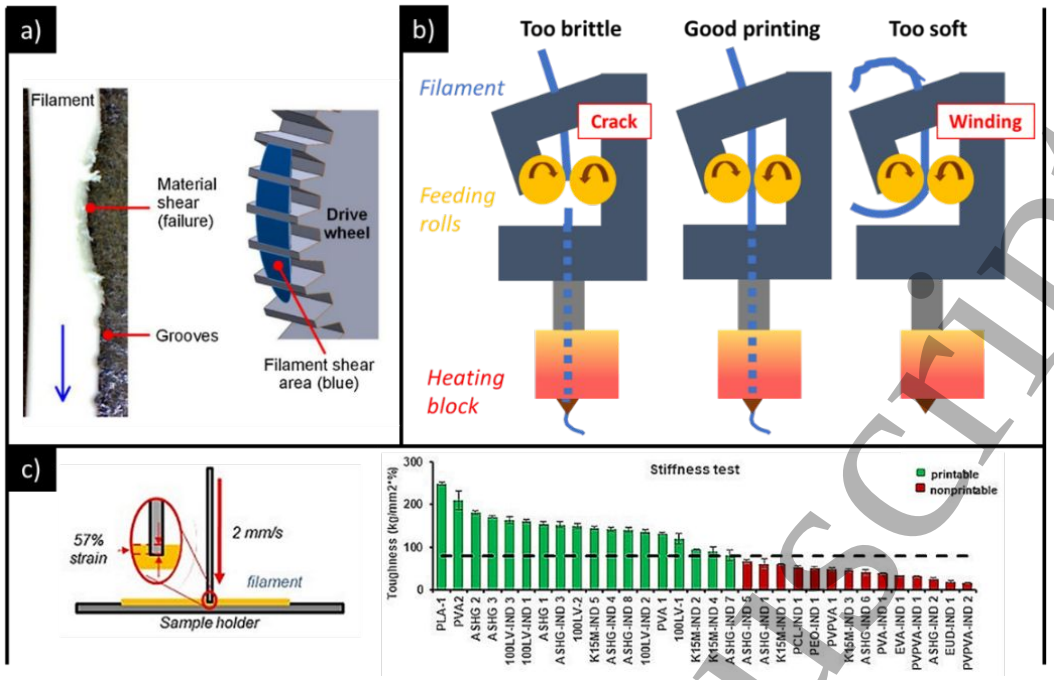

Figure 20 (a) Filament shear failure reproduced from (135) with permission of © 2017 Elsevier Inc (b) Feeding issues linked to filament mechanical properties adapted from(134) (c) Correlation between stiffness result and printability for different formulations of drugs loaded filament reproduced from (138) with permission of © 2020 Elsevier

Rheological and thermal properties suitable to the process are needed to allow the flow of polymers through the nozzle. FFF3D printing is a non-continuous extrusion process that induces shear rate fluctuations changing the viscosity of the melt (139). Beran *et al.* (136) have modified the printing speed from 20 mm.s^{-1} to 70 mm.s^{-1} and they found the equivalent shear rate between 2x10^{2} and 6x10^{2} s^{-1}. According to Arrigo and Frache (137), the printing of a 1.75mm diameter filament, with a 0.4mm nozzle at 30mm.s^{-1}, corresponds to a shear rate between 9x10^{2} and 2x10^{3} s^{-1}. They have investigated rheological properties required for FFF printing by studying: **flowability, filament buckling, shape stability, die swelling, and interlayer adhesion**. Non-Newtonian characteristics are beneficial for printing with a low melt viscosity during the flow through the nozzle that increases rapidly when the material exits (zero-shear conditions). It contributes to reduce buckling risk (136) as well as it permits to avoid dripping during the non-printing movement. For Samoro *et al.* (139), high melt viscosity is a drawback for the constant flow during the printing of drug-loaded filament. However, non-Newtonian features provide swelling when materials exit the nozzle so optimized printing parameters are needed (133). As printing involves heating, melting, and solidifying, convenient thermal properties with a sufficient content of thermoplastic are needed (139). For instance, the incomplete relaxation of polymer chains during cooling will affect negatively the welding of each layer(137). Dries Vaes and Peter Van Puyveld (140) have studied FFF printing of semi-crystalline polymers. For these polymers, a drop-in viscosity happens when the melting point temperature is jumped over. A minimal heat transfer is required to lower polymers' viscosity to avoid higher extrusion forces and nozzle clogging (140). It intensifies at higher print speeds which also induces higher extrusion force due to a reduced residence time of the extruded material in the heating block. The maximal extrusion force, which is around 60 N for a classical 3D printer, can be exceeded leading to printing failure (135).

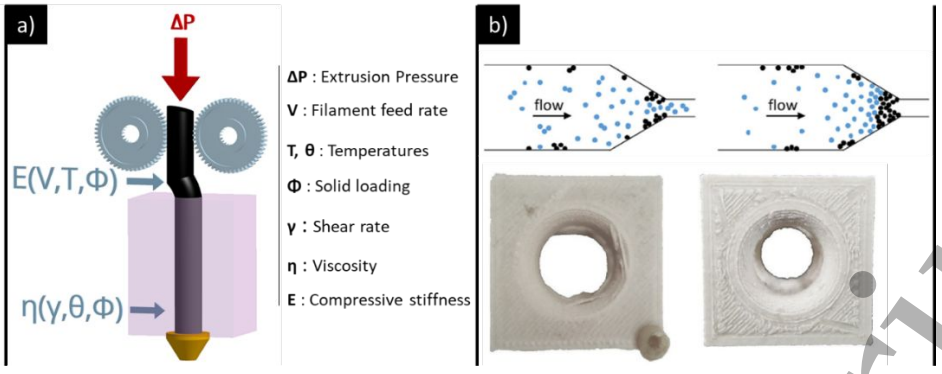

Figure 21 (a) Schematic of buckling issue with involved parameters, (b) Clogging with loaded filament. Polycarbonate with 30 vol% and 40 vol% of glass spheres successfully printed, reproduced with permission from (136)

For battery printing applications, researchers have tried to decrease the content of hosting polymer (from 80 wt%(35) to 46 wt%(27)) to maximize electrochemical performances of printed filament. However, fillers have an impact on mechanical and rheological behavior. Beran and coworkers (136) have studied the printability of loaded filaments. A decrease lower than 50 vol% of hosting polymer hampers the filament's printability. Depending on the size and shape of fillers, it could generate clogging during printing. An increase in size results in higher viscosity and therefore the use of a larger nozzle when printing. For a ratio nozzle diameter/filler size lower than 6.2, they have observed systematic clogging of the filament (136) [fig. 21(b)]. However, a larger nozzle induces higher printing layer height and thus a lower resolution. They conclude that the printability is influenced by the filler volume content, the zero-shear viscosity of the matrix, and printer conditions (printer speed and temperature). In their study on FFF printing of a glass spheres-filled polycarbonate filament through a 0.4 mm nozzle, they have established a viscosity criterion on the zero-shear viscosity of the matrix. Moreover, Verstraete and coworkers (134) have worked on drugs-loaded thermoplastic polyurethane (TPU) filament for FFF printing for the pharmaceutical domain. They investigated the impact of the roughness and variation of filament diameter induce by fillers, which can be the origin of printability issues.

2. Microgravity environment specifications

For the last 10 years, space agencies have worked to develop on-orbit additive manufacturing facilities. Polymer printing by stereolithography (SLA) or FFF, and metal printing are the main studied processes. Major achievements related to additive manufacturing by FFF process suitable for microgravity or being operated in microgravity are reported in Table 2. Several suitable 3D printers have been developed to process a range of thermoplastics in microgravity and 3D printed parts have already been manufactured onboard the ISS. Moreover, 3D printing using continuous carbon fiber reinforced PLA composites in space has been achieved by Chinese research institutes on board spacecraft (141).

Country	Date	Project	Materials	State	Ref
USA	2014	3DP	ABS	Flight ISS	(6)
Italy	2015-2016	POP3D	PLA	Flight ISS	(7)
Europe	2015-2018	MELT	PEEK	Ground	(142)
USA	2016-to date	AMF	ABS / PEI / HDPE	Flight ISS	(143,144)
USA	2019	REFABRICATOR	Ultem®	Flight ISS	(145)
Europe	2019-2021	IMPERIAL	PEEK / Ultem®	Ground	(146)
China	2020	-	PLA + continuous carbon fibers	Flight (spacecraft)	(10,141)

Table 2 List of FFF 3D printers operated in and developed for the microgravity environment

It is clear from the list of successful projects mentioned [Tab. 2] that this process is fully compatible with a microgravity environment leading to the manufacturing of parts with comparable properties as one manufactured under earth gravity (6,7). So far, the FFF process in orbit has been demonstrated to be stable and efficient. Full process automation is implemented, and the reliability of such 3D printers as well as printing parameters are thoroughly assessed to minimize the need for human intervention besides printed part recovery. The range of polymers used spans from commodity (PLA/ABS) to high-performance thermoplastics (PEEK / polyetherimide (PEI)-based Ultem®). Looking at the range of material processed so far, microgravity-compatible 3D printers are capable of reaching extrusion temperature at least compatible with Ultem® and PEEK (~380 °C).

From the available literature, all specific printing parameters used that enable the fine-tuning of the printing process as a function of the polymer are not disclosed. The 3DP project used ABS and a 0.4 mm diameter nozzle. In the POP3D project that used PLA, the printing temperature was set between 160 and 180 °C with an average flow rate between 1 to 10 mm^3/s (7). For the MELT project focusing on PEEK, a 0.4 mm nozzle was used with a temperature of 380 °C and a printing speed of 20 mm/s (142). The IMPERIAL project has assessed the capability to 3D print parts with no size limitation in one direction of the build volume with an extrusion temperature of 400 °C, and heated chamber at 100 °C in order to process PEEK and Ultem®.

To implement such a process under microgravity, there are several key aspects to consider that are linked to the fine-tuning of the printing parameters considering the printer design (nozzle diameter, heating capability, motor accuracy…) and the intrinsic material properties (melting temperature, melt flow index). The first one is the feedstock shape and how the material in its solid state is fed to the extruder to enable the melting process. Most of the experiments performed so far have used filaments that are stored in spools. This implies that the filament of the feedstock needs to exhibit a certain flexibility to be able to be rolled around the spool and later unrolled without any irreversible deformations (bending, kinking, breaking) that might hamper or block the feeding process. Therefore, very stiff filament or composite filament highly loaded with filler might present issues in reaching the desired radius of curvature to be stored in a spool of a convenient diameter. For the feeding process, the potential issues described in Table 3, must be avoided to enable a good feeding process with a continuous and controlled flow of material in the nozzle but also to avoid any human intervention or need for extensive maintenance by operators. It is of utmost importance to underline that in orbit, astronaut crew time is very limited and needs to be efficiently used with respect to their mission; any loss of this time to solve such issues will be negatively affecting the efficiency of such process and its overall added value.

On-orbit FFF 3D printing imposes additional constraints compared to on-earth manufacturing. The confined environment of a space station hinders the use of highly volatile species. Safety requirements of the ISS, establish a toxicity hazard level (THL) (from 1 to 4) according to volatility and the hazardous nature of chemical species (147). Even if, all 3D printers are operating in a closed environment including venting and filtering capabilities, it is highly recommended to select materials with low-volatility chemicals. Battery electrolytes are considered to be THL-2 or higher. There are also stringent rules on flammable materials to eliminate fire propagation issues in the ISS environment. The lack of gravity makes the use of fluid critical, especially in the case of wetting a porous media. Particles rearrangements and separations can accentuate wetting instabilities (148).

In summary, the compliance of the FFF process with microgravity is due to a compliant surface tension of melted thermoplastic and its viscosity that enables the melt pool to be extruded and adhere to a primary surface. From these achievements so far one can conclude that any thermoplastics that can find similarities with the ones described in Table 2 could be processed efficiently under a microgravity

environment. In this respect, the most important parameters to be assessed when it comes to new materials are related to the feedstock mechanical properties for the nozzle feeding process (feedability), the achieved viscosity, shear rate, and pressure during the melting process (rheology) (149) and finally the limits imposed by the 3D printer design in term of printing volume, accuracy, and versatility (multi-material possibility, ease of operation…).

3. Suitable strategies for PE printing in microgravity

FFF 3D printing specifications are not compatible with all polymer electrolyte strategies [Tab. 3]. A minimum amount of thermoplastic polymer is required to meet rheological and mechanical features which is not the case for **polymer-in-salt and polymer-in-ceramic** strategies. Thus, these strategies are considered unfavorable regarding their rheological behavior. **Quasi-solid electrolytes** and **salt-in-polymer electrolytes** display issues of feedability because of their lack of mechanical stability and stiffness. For instance, difficulties in printing a PEO:LiTFSI 20:1 electrolyte have been illustrated by Maurel and coworkers (24). The sticky filament did not provide enough hardness to be printed with classical printer configuration. In highly plasticized polymer electrolytes, organic solvent volatilization during extrusion, printing, and storage can degrade the mechanical behavior of the filament. For instance, filaments containing PEGDME200 and acetyl tributyl citrate (ATBC), tend to exude plasticizer and become fragile under atmospheric conditions and room temperature, even if reported boiling points are higher (327°C for ATBC) (150). That is why the use of a volatile plasticizer to have a more flexible filament is a short-term solution(139). Like other strategies involving volatile chemical species, it is strongly going against the above-mentioned safety requirements of the ISS even if mitigation could be implemented due to the availability of a venting line and having a printer hermetically closed. Every strategy with a score lower than 3/5 on Figure 19, has been classified as unfavorable for mechanical reasons. Polymer-in-ceramics are also unfavorable due to their high stiffness. In terms of morphology, filament extrusion followed by FFF printing involves the melting of species at different temperatures and shear rates. It results in specific anisotropic morphologies, influenced by many parameters (extrusion and printing parameters, polymers rheological behavior) (140). **Gel polymer electrolytes**, **controlled nanostructured channels, interpenetrating networks, and crosslinking polymer** solutions are feasible only if the morphology can be controlled all along the process. Indeed, gel polymer electrolytes require entrapped liquid phases, and crosslinked polymer electrolytes are mainly manufactured by thermal decomposition which is not compatible with extrusion. Thus, entrapped liquid phases, nanostructured channels, and photo-initiated crosslinking of polymers are considered infeasible by a double extrusion process. That is why they are regarded as unfavorable strategies for morphology issues.

	FFF specifications / PE strategies	Printability *(Rheology)*	Feedability *(Mechanics)*	Feasability *(Morphology)*	*Assessment*
QSPE	Gel Polymer Electrolyte (GPE)				X
	Polymeric Ionic Liquid Electrolyte (PILE)				X
	Highly plasticized polymer				X
	Polymer-in-salt				X
CPE	Ceramic-in-polymer				OK
	Polymer-in-ceramic				X
	Salt-in-polymer				X

SPE	Polymer blend				OK
	Single Ion Polymer Electrolyte (SIPE)				OK
	Crosslinking Polymer				X
	Copolymer electrolytes				X
	Multilayered electrolytes				OK
	Nanostructured electrolytes				X
	Inter-Penetrating Network (IPN)				X

Table 3 Compatibility of polymer electrolyte strategies with FFF 3D printing process (red=unfavorable / green=favorable)

With these considerations, four residual strategies appear suitable to print polymer electrolytes by the FFF process. **Multilayered electrolyte** strategy requires different filaments to realize the 3D printing which makes the process in case of multi-material printing more complicated. Additional printing heads would be needed to avoid the use of two filaments with the same nozzle which requires cleaning steps. Such multilayered electrolyte exhibits lower ionic conductivity but offers added value in high-potential energy storage applications. It is the same for the **single-ion strategies**. It reduces the polarity of the cell without displaying the best ionic conductivities at room temperature (88). This strategy is especially interesting for LMB as it permits to prevent dendritic growth. **Copolymer solutions** are promising strategies requiring important chemistry steps to suit extrusion and 3D printing.

With these assumptions regarding process conditions and microgravity environment, polymer blending and composite polymer electrolyte are the two remaining strategies suitable for the 3D printing of Li-ion polymer batteries by FFF in a microgravity environment.

Polymer blend electrolytes by FFF: . Immiscible blends can offer complementary features that can be studied with two polymers: polymer A, containing Li salt, serves as a Li^+ pathway with a poor mechanical behavior; polymer B, chemically inert, acts as mechanical reinforcement. It could improve ionic conductivity by:

1. Reducing the crystallinity rate thus increasing segmental mobility in phase A
2. Increasing the lithium salt content at an optimized rate in phase A, without degrading the overall mechanical behavior thanks to the mechanical compensation of B
3. Creating preferential pathways of Li^+ through phase A thanks to the resulting morphology

The choice **of polymers, salt** and **proportion** (Polymer A: Polymer B: Li salt) are key parameters. An increase in polymer B content would enhance overall filament stiffness, but would decrease the volume proportion of the conducting phase, which could degrade the ionic conductivity. On the opposite, an increase in Li salt content could enhance ionic motion while plasticizing the filament. **Process parameters** (extrusion and 3D printing processes parameters) have also a major influence on electrolyte performances. In this double extrusion process, temperatures and shear rate affect the morphology, by influencing the viscosity and crystallinity rate, which are two key parameters of ionic motion. Extrusion temperatures must be between the melting and the degradation points of polymers. Indeed, they must be processable in the same range of temperature (151). The speed and rotating mode (co-rotative or counter-rotative) of the screw will modify the applied shear rate. A minimal shear rate is needed to ensure the complete melting of polymers as well as the good homogeneity of the blend. However, a too high shear rate, as well as a too high temperature, lead to polymer degradations. Verdier et al. have underlined PEO degradations above 135°C during extrusion. According to them, polymer degradations should always be considered when the extrusion process is used (151). 3D printing, as a discontinuous extrusion step, also impacts crystallinity and morphology as shown by Vaes and Puyvelde (140) in their review. It depends on printing parameters (liquefier temperature, bed

temperature, printing speed and strategy) and the type of polymer. Temperature should be high enough to lower the viscosity and avoid filament buckling in the upper part of the printing head. Heated bed and chamber influence the recrystallization and tend to increase the crystallinity rate (152). The ionic conductivity of the 3D printed electrolyte could be improved by a drop of crystallinity provided by a fast cooling (high fan speed and low bed temperature). Polymer degradations are also supposed to happen during printing. Finally, printing strategies should be considered due to the anisotropic morphology of printed parts. In biphasic filament morphology, an elongation of domains along the printing direction can be observed (140). Moreover, macro porosities are visible inside FFF 3D printed parts (153). All of these parameters will modify the viscosity of each phase which has an impact on tortuosity and accessibility of the ionic conductive phase [fig. 22]. A fine-tuning these parameters is needed to obtain a trade-off between mechanical and electrochemical properties. Petra Potschke and coworkers have investigated co-continuous structure formation in an immiscible blend (154). The co-continuity mainly depends on the viscosity ratio and volumetric phase proportion. Thus, a precise process condition permits to find the inversion phase point at which the co-continuity is reached. Several empirical models have been proposed to describe the phenomenon with a common point of co-continuity at the equivolume and equiviscous point. A co-continuous structure permits a maximal contribution of the mechanical modulus from polymer B while ensuring a continuous pathway for Li^+ in polymer A.

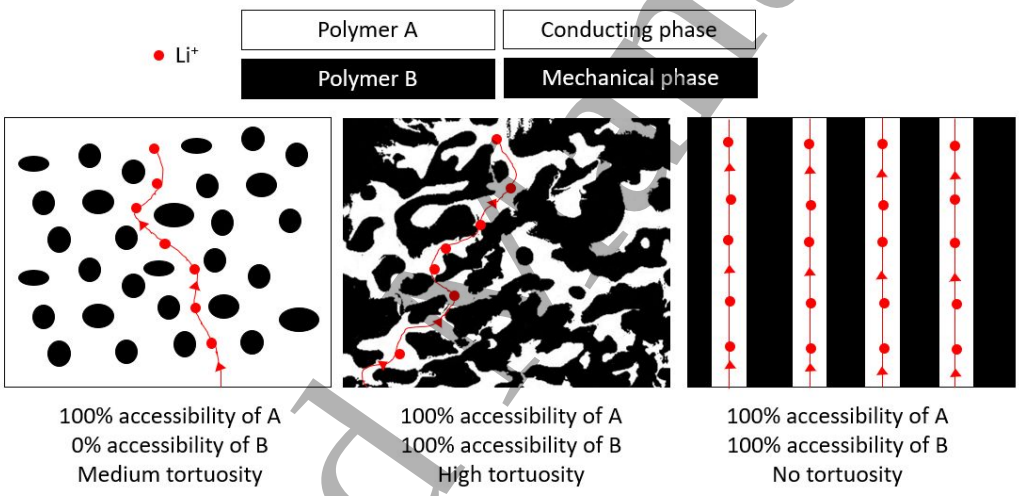

Figure 22 Morphology of an immiscible polymer blend

Composite electrolyte by FFF : This strategy involves a polymer A, which conveys Li^+ and fillers, passive or active. In the case of passive fillers, the aim is to avoid filler aggregations, and homogenize filler dispersion in the polymer matrix to enhance the mechanical behavior of the filament and reduce crystallinity. Thus, process parameters such as higher shear rates and temperatures contribute to homogenizing the particle's repartition in the polymer. The sequencing is important in this case. For instance, fillers and polymers premixed without Li salt can favor polymer-filler interactions to avoid aggregation. In the case of active fillers, percolation of particles is required to leverage their high ionic conductivity. If the percolation threshold is overcome, it could improve the ionic conductivity by opening new pathways through inorganic particles. However, more than 40 wt% of fillers would hinder the printability. Thus, it is necessary to lower the percolation threshold to benefit from the filler's ionic conductivity without compromising the printability. An immiscible co-continuous polymer blend can be used to confine particles inside one phase or at the interface. Plattier and coworkers have confined carbon black particles at the interface of a co-continuous blend of PP and poly-ε-caprolactone (PCL) thanks to a viscosity ratio close to one (155). Shear rate and temperature during extrusion and printing, as well as polymer proportions control fillers localization by modifying viscosities. The 3D printing of

CPE, based on inactive fillers, has already been studied. 1 wt% SiO_2 starts to decrease crystallinity and permits improved printability (38). Mejia *et al.* (156) have extruded an electrolyte composed of PEO ($Mn=5x10^6$)/LiTFI (EO:Li=12:1) with additional D-α-tocopherol polyethylene glycol 1000 succinate (TGPS)-coated sepiolite nanofibers (up to 15 nm). It was found that the latter favored mechanical behavior by creating a 3D network of PEO. The ionic conductivity was close to 10^{-3} S.cm^{-1} at 25°C with a solid-like behavior that makes it extrudable. However, they have used 40 wt% of ethylene carbonate (EC) to highly plasticize their electrolyte which explains the reached ionic conductivity. To avoid the use of EC with its low electrochemical and thermal stability, they have replaced it with a less volatile ionic liquid, $PYR_{14}TFSI$. However, the ionic conductivity was reduced by an order of magnitude (157). Two recent papers demonstrate the solvent-free manufacturing and extrusion feasibility of composite electrolytes based on active fillers. Zhen Li *et al.* have used extrusion to create an electrolyte membrane of PEO/LiTFSI filled with 75 wt% of LLTO. This extrusion method with a high content of ceramics provides a tensile strength 3 times higher than that of the solution casting method and a transference number 5 times higher than that of PEO/LiTFSI. However, it portrays an ionic conductivity of $2.95x10^{-5}$ S.cm^{-1} at 30°C and a high interfacial resistance (111). Moreover, such loadings are not suitable for FFF 3D printing. A PEO/LiTFSI electrolyte filled with low loading (10 wt% of LLZTO nanoparticles) has been manufactured by solvent-free hot rolling. It exhibits a similar ionic conductivity of $6.8x10^{-5}$ S.cm^{-1} at 30°C (68).

4. Residual challenges

The main challenge towards Li-ion polymer battery printing is the polymer electrolyte manufacturing, which is non-trivial due to a strong opposition between mechanical et electrochemical properties. However, it is not the only challenge to take up so as to 3D print by FFF full polymer batteries. Complementary to this major issue, the following residual challenges stand in the way in terms of all-solid-state cell assembly, process conditions, and performances optimization.

- **All-solid-state assembly:**

Electrodes: In all-solid-state batteries, the ionic transport from the electrolyte interface to the active material located in electrodes is difficult to achieve. The need for clear pathways up to active material makes the presence of solid electrolyte inside electrodes necessary. Thus, improvement of energy density and coulombic efficiency could be obtained by replacing traditional electrode binders with polymer electrolyte formulation (157). Ragones and coworkers (38) made the hypothesis that their low capacity and sloping charge/discharge profiles were linked to the absence of Li salt and PEO in their printed PLA-based electrodes. Aldalur *et al*. (158) have used a new formulation of amorphous polymer electrolyte based on (propylene oxide (PO)/EO) Jeffamine ($4x10^{-5}$ S.cm^{-1} at 25°C) as a binder in the cathode with LFP (over 150 cycles).

Casing protects active parts of the battery. It must have high mechanical and thermal stability, good adhesion with all the parts, and be chemically and electrically inert. PEEK, nylon, or reinforced filament with fiberglass are therefore good candidates even if they required more stringent 3D printing parameters. Low porosity is also important to ensure the impermeability of the casing. Printing temperatures for the casing have to be chosen not to degrade other filaments. A thermal gradient can also affect the crystallinity and morphology of other filaments which will have an effect on electrochemical properties.

Interfaces: Contact at interfaces are a major concern in the case of all-solid-state batteries. Solid-solid interfaces provide a higher resistance that hinders Li^+ motions through interfaces. Behavior at interfaces with electrolytes/electrodes must be studied. Interlayer adhesion can provide good contact

between each electrode and the electrolyte but might be impacted by the microgravity environment. Process temperatures and cooling behavior must be compatible with each filament.

- **Process conditions requirements**.

Dry environment: Lithium salt and some polymers are highly hygroscopic species. Extrusion and printing steps have to occur in a low humidity-controlled environment to avoid a drop-in viscosity and degradation of the filament mechanical stability.
Multi-material printing: As one-shot printing involves a different feedstock for each part of the battery, it is important to avoid any contamination during the process. Residual conductive or active materials in the printing head can cause short-circuit. Several answers have been imagined to overcome filament pollution. Cleaning sequence with an inert material will increase the manufacturing time. Multi-material printers with one printing head for each filament would permit a one-shot 3D printing while reducing the pollution of each part by another one.
Printing parameters optimization: temperatures, speed of printing, cooling rate or layer height are parameters which can affect the quality of printing and battery electrochemical performances (33).
Greener processes: Extrusion and 3D printing are good candidates to be solvent-free methods of manufacturing. Removing hazardous solvents as well as limiting the use of nanopowders are key factors to ensure safer working conditions.
Microgravity environment: In case microgravity is part of the printing environment, there are a few uncertainties concerning the use of filled thermoplastics and their homogeneity after being melted and extruded. Microgravity may induce local changes in the filler content, dispersion, and homogeneity within the printed material creating a gradient within one deposited layer. If such an effect leads to a decrease of filler content at the interface, printing will have an impact on the overall ionic conductivity by forming, at the microscopic level, a gradient of properties that will differ from the bulk material properties.

- **Electrochemical performances optimization**

3D architecture: Optimized architecture could permit to make up for energy density loss induced by the large proportion of thermoplastic. Modeling studies could help to design more efficient batteries with larger specific areas.
High potential materials: The majority of studies choose LTO and LFP as negative and positive electrode materials, respectively, because of their low volumetric expansion and thermal stability (29). An increase in efficiency could be brought by studying 3D printing of higher potential cathode material such as NMC for the cathode. It will bring new challenges for cathode 3D printing as NMC particles can be bigger than LFP which could create issues of polymer coating and filament homogeneity which can impact cell performances. Concerning electrolytes, higher potential means side reactions with polyether such as PEO. That is why electrochemically stable polymers have to be explored even if they provide less ionic conductivity and low-potential stability.

Conclusion

On the one hand, FFF printing has been successfully implemented on orbit and onboard the International Space Station, which demonstrates its suitability for a microgravity environment. The target is to be able to answer astronauts' vital needs for future long-mission, by manufacturing on-demand, tailorable, and complex items directly in space decreasing the need for spare parts brought from Earth. On the other hand, FFF is a new promising manufacturing process for energy storage devices. Its freedom of design and ease of process could permit a reduction in cost and time of production. During the last 5 years, FFF 3D printing of electrodes, separators, and current collectors for Li-ion batteries have been studied with promising results. However, these cells still need to be impregnated with hazardous and volatile liquid electrolytes. Thus, solid polymer electrolyte printing represents the main challenge to take up towards one-shot printing of LIB in microgravity. Up to now, two groups have already 3D printed electrolytes by FFF, however facing printability issues (24) or reaching ionic conductivity 10^{-5} S.cm^{-1} at 60°C that are low compared to the needs (38). Indeed, Li^+ motion mechanisms in polymers are non-trivial and their semi-crystallinity makes them inefficient at room temperature. Several strategies have been investigated to overcome these issues. We can gather them into three main categories: Quasi-solid Polymer Electrolytes (QSPE), Composite Polymer Electrolytes (CPE), and Solid Polymer Electrolytes (SPE). QSPEs suffer from poor mechanical behavior, and some strategies from CPE or SPE groups require specific morphologies or a huge amount of fillers. That is why, facing FFF 3D printing mechanical, rheological, and morphological specifications, most of electrolyte strategies are incompatible with the process. Moreover, solutions involving volatile, flammable, or hazardous species are not suitable for the safety requirements of the confined environment of a space station. Among feasible solutions, SPE with polymer blend and CPE seem to represent the best way to successfully 3D prints an electrolyte compatible with a microgravity environment. The main parameters which are materials choice, materials proportion, and extrusion/printing parameters have to be optimized to enhance ionic conductivity without degrading the mechanical behavior. In the case of CPE, active fillers are attractive to improve this ionic conductivity especially if they can be confined in a continuous network. Thus, the polymer blend strategy could be used to confine active fillers in one phase or at the interface between the two domains by playing with the sequencing, viscosities, and wetting coefficients. Future studies could be performed on copolymer strategy which could be an efficient method but it requires chemical synthesis of a particular polymer able to convey Li cations and be processable in a double extrusion process at the same time. On the process side, the utilization of Direct Extrusion Additive Manufacturing (DEAM) (139) should be worth considering as it would avoid the use of filament as feeding materials at the origin of strong mechanical constraints. It could bring formulation freedom by directly feeding the printer with pellets or powder and it has not been investigated yet for Li-ion battery manufacturing. To conclude solvent-free polymer electrolyte 3D printing by FFF is the crucial step to open the way toward one-shot Li-ion polymer battery printing in a microgravity environment.

Acknowledgement

This work was supported by the Région Hauts-de-France, the European Space Agency (ESA) and the University of Picardie Jules Verne (UPJV). It was performed in the frame of ESA Contract 4000139673.

References

1. Creech S, Guidi J, Elburn D. Artemis: An Overview of NASA's Activities to Return Humans to the Moon. In: 2022 IEEE Aerospace Conference (AERO). 2022. p. 1‑7.

2. Leach N. 3D Printing in Space: 3D Printing in Space. Archit Design. nov 2014;84(6):108‑13.

3. Makaya A, Pambaguian L, Ghidni T, Rohr T, Lafont U, Meurisse A. Towards out of earth manufacturing: overview of the ESA materials and processes activities on manufacturing in space. CEAS Space Journal. mars 2022;

4. Labeaga-Martínez N, Sanjurjo-Rivo M, Díaz-Álvarez J, Martínez-Frías J. Additive manufacturing for a Moon village. Procedia Manufacturing. 2017;13:794‑801.

5. Terfansky M, Thangavelu M, Fritz B, Khoshnevis B. 3D Printing of Food for Space Missions. AIAA SPACE Forum [Internet]. 2013 [cité 6 juin 2023]; Disponible sur: https://arc.aiaa.org/doi/10.2514/6.2013-5346

6. Prater T, Werkheiser N, Ledbetter F, Timucin D, Wheeler K, Snyder M. 3D Printing in Zero G Technology Demonstration Mission: complete experimental results and summary of related material modeling efforts. Int J Adv Manuf Technol. mars 2019;101(1‑4):391‑417.

7. Musso G, Lentini G, Enrietti L, Volpe C, Ambrosio EP, Lorusso M, et al. Portable on Orbit Printer 3D: 1st European Additive Manufacturing Machine on International Space Station. Goonetilleke R, Karwowski W, éditeurs. Advances in Physical Ergonomics and Human Factors. 2016;489:643‑55.

8. Space MI. New Space-Based Manufacturing Technologies Demonstrated by Made In Space [Internet]. Made In Space. 2017 [cité 6 juin 2023]. Disponible sur: https://medium.com/made-in-space/new-space-based-manufacturing-technologies-demonstrated-by-made-in-space-79000e771ac4

9. Zocca A, Wilbig J, Waske A, Günster J, Widjaja MP, Neumann C, et al. Challenges in the Technology Development for Additive Manufacturing in Space. Chinese Journal of Mechanical Engineering: Additive Manufacturing Frontiers. 1 mars 2022;1(1):100018.

10. Huaxia. Xinhuanet. 2020 [cité 15 sept 2023]. China Focus: China tests 3D printing in space for first time. Disponible sur: http://www.xinhuanet.com/english/2020-05/09/c_139043524.htm

11. Julielynn Y. Wong. 3D printing Applications for Space missions. Aerospace Medicine and Human Performance. juin 2016;87(6):580‑2.

12. Maurel A, Martinez AC, Dornbusch DA, Huddleston WH, Seol ML, Henry CR, et al. What Would Battery Manufacturing Look Like on the Moon and Mars? ACS Energy Lett. 20 janv 2023;1042‑9.

13. Owens A, De Weck O. Systems Analysis of In-Space Manufacturing Applications for the International Space Station and the Evolvable Mars Campaign. AIAA SPACE 2016. 9 sept 2016;AIAA SPACE Forum(AIAA 2016-5394).

14. Tarascon JM, Armand M. Issues and challenges facing rechargeable lithium batteries. Nature. nov 2001;414(6861):359‑67.

15. HULL CW. Apparatus for production of three-dimensional objects by stereolithography. US4575330A. 1986;

16. Kiran ASK, Veluru JB, Merum S, Radhamani AV, Doble M, Kumar TSS, et al. Additive manufacturing technologies: an overview of challenges and perspective of using electrospraying. Nanocomposites. 2 oct 2018;4(4):190‑214.

17. Criado-Gonzalez M, Dominguez-Alfaro A, Lopez-Larrea N, Alegret N, Mecerreyes D. Additive Manufacturing of Conducting Polymers: Recent Advances, Challenges, and Opportunities. ACS Appl Polym Mater. 11 juin 2021;3(6):2865‑83.

18. (Dogan) Baydogan N, Ponnada S, Gorle D, Bose RSC, Kiai M, Devi M, et al. Current Insight into 3D Printing in Solid-State Lithium-Ion Batteries: A Perspective. Batteries & Supercaps. 7 juin 2022;

19. Lau KT, M.T. M, Rashid N, Manogaran D, Ahmad M. EFFECT OF HBN FILLERS ON RHEOLOGY PROPERTY AND SURFACE MICROSTRUCTURE OF ABS EXTRUDATE. Jurnal Teknologi. 30 mai 2022;84:175‑82.

20. Ambrosi A, Pumera M. 3D-printing technologies for electrochemical applications. Chem Soc Rev. 17 mai 2016;45(10):2740‑55.

21. Materials AS for T. Standard Terminology for Additive Manufacturing Technologies: ASTM F2792-12A. ASTM International; 2012. book.

22. Yang Y, Yuan W, Zhang X, Yuan Y, Wang C, Ye Y, et al. Overview on the applications of three-dimensional printing for rechargeable lithium-ion batteries. Applied Energy. 1 janv 2020;257:114002.

23. Lyu Z, Lim GJH, Koh JJ, Li Y, Ma Y, Ding J, et al. Design and Manufacture of 3D-Printed Batteries. Joule. 20 janv 2021;5(1):89‑114.

24. Maurel A, Armand M, Grugeon S, Fleutot B, Davoisne C, Tortajada H, et al. Poly(Ethylene Oxide)−LiTFSI Solid Polymer Electrolyte Filaments for Fused Deposition Modeling Three-Dimensional Printing. Journal of The Electrochemical Society. 2020;167(070536).

25. Pei M, Shi H, Yao F, Liang S, Xu Z, Pei X, et al. 3D printing of advanced lithium batteries: a designing strategy of electrode/electrolyte architectures. J Mater Chem A. 23 nov 2021;9(45):25237‑57.

26. Wang J, Sun Q, Gao X, Wang C, Li W, Holness FB, et al. Toward High Areal Energy and Power Density Electrode for Li-Ion Batteries via Optimized 3D Printing Approach. ACS Appl Mater Interfaces. 21 nov 2018;10(46):39794‑801.

27. Maurel A, Grugeon S, Fleutot B, Courty M, Prashantha K, Tortajada H, et al. Three-Dimensional Printing of a LiFePO4/Graphite Battery Cell via Fused Deposition Modeling. Sci Rep. 2 déc 2019;9(1):18031.

28. Ragones H, Menkin S, Kamir Y, Gladkikh A, Mukra T, Kosa G, et al. Towards smart free form-factor 3D printable batteries. Sustainable Energy Fuels. 26 juin 2018;2(7):1542‑9.

29. Huifa S, Jiakai C, Zhenhua S, Ali Ghazi Z, Zhu X, Han S, et al. 3DPrinting Enables Customizable Batteries. Batteries & Supercaps. 2023;

30. Reyes C, Somogyi R, Niu S, Cruz MA, Yang F, Catenacci MJ, et al. Three-Dimensional Printing of a Complete Lithium Ion Battery with Fused Filament Fabrication. ACS Appl Energy Mater. 22 oct 2018;1(10):5268‑79.

31. Sun K, Wei TS, Ahn BY, Seo JY, Dillon SJ, Lewis JA. 3D Printing of Interdigitated Li-Ion Microbattery Architectures. Advanced Materials. 2013;25(33):4539‑43.

32. Chen Q, Xu R, He Z, Zhao K, Pan L. Printing 3D Gel Polymer Electrolyte in Lithium-Ion Microbattery Using Stereolithography. J Electrochem Soc. 30 juin 2017;164(9):A1852.

33. Maurel A, Grugeon S, Armand M, Fleutot B, Courty M, Prashantha K, et al. Overview on Lithium-Ion Battery 3D-Printing By Means of Material Extrusion. ECS Trans. 8 sept 2020;98(13):3.

34. Zhang D, Chi B, Li B, Gao Z, Du Y, Guo J, et al. Fabrication of highly conductive graphene flexible circuits by 3D printing. Synthetic Metals. 1 juill 2016;217:79‑86.

35. Foster CW, Down MP, Zhang Y, Ji X, Rowley-Neale SJ, Smith GC, et al. 3D Printed Graphene Based Energy Storage Devices. Sci Rep. 3 mars 2017;7(1):42233.

36. Vinegrad A, Ragones H, Jayakody N, Ardel G, Goor M, Kamir Y, et al. Plasticized 3D-Printed Polymer Electrolytes for Lithium-Ion Batteries. J Electrochem Soc. nov 2021;168(11):110549.

37. Maurel A, Kim H, Russo R, Grugeon S, Armand M, Panier S, et al. Ag-Coated Cu/Polylactic Acid Composite Filament for Lithium and Sodium-Ion Battery Current Collector Three-Dimensional Printing via Thermoplastic Material Extrusion. Frontiers in Energy Research [Internet]. 2021 [cité 1 mars 2023];9. Disponible sur: https://www.frontiersin.org/articles/10.3389/fenrg.2021.651041

38. Ragones H, Vinegrad A, Ardel G, Goor M, Kamir Y, Dorfman MM, et al. On the Road to a Multi-Coaxial-Cable Battery: Development of a Novel 3D-Printed Composite Solid Electrolyte. J Electrochem Soc. 3 déc 2019;167(7):070503.

39. Mindemark, J. Lacey M, Bowden T, Brandell D. Beyond PEO—Alternative host materials for Li+-conducting solidpolymer electrolytes. Progress in Polymer Science. 2018;

40. Wright PV. Polymer electrolytes—the early days. Electrochimica Acta. 30 avr 1998;43(10):1137‑43.

41. Armand MB. Polymer Electrolytes. Annual Review of Materials Science. 1986;16(1):245‑61.

42. Blue Solutions. ELECTROLYTE FOR LITHIUM POLYMER BATTERIES [Internet]. [cité 30 mai 2023]. Disponible sur: https://worldwide.espacenet.com/patent/search/family/040789043/publication/US2020295395A1?q=pn%3DUS2020295395A1

43. Hallinan DT, Balsara NP. Polymer Electrolytes. Annu Rev Mater Res. 1 juill 2013;43(1):503‑25.

44. Xu X, Hui KS, Hui KN, Wang H, Liu J. Recent Advances in the Interface Design of Solid-State 2 Electrolytes for Solid-State Energy Storage Devices. Materials Horizons. 2020;

45. Barbosa JC, Gonçalves R, Costa CM, Lanceros-Méndez S. Toward Sustainable Solid Polymer Electrolytes for Lithium-Ion Batteries. ACS Omega. 3 mai 2022;7(17):14457‑64.

46. Fergus JW. Ceramic and polymeric solid electrolytes for lithium-ion batteries. Journal of Power Sources. août 2010;195(15):4554‑69.

47. Ratner MA, Johansson P, Shriver DF. Polymer Electrolytes: Ionic Transport Mechanisms and Relaxation Coupling. MRS Bull. mars 2000;25(3):31‑7.

48. Meng N, Lian F, Cui G. Macromolecular Design of Lithium Conductive Polymer as Electrolyte for Solid-State Lithium Batteries. Small. 2021;17(3):2005762.

49. Caradant L, Verdier N, Foran G, Lepage D, Prébé A, Aymé-Perrot D, et al. Extrusion of Polymer Blend Electrolytes for Solid State Lithium batteries. ACS Applied Polymer Materials. 2021;

50. Vincent CA. Polymer electrolytes. Progress in Solid State Chemistry. 1 janv 1987;17(3):145‑261.

51. Szcesna-Chrzan A, Marczewski M, Syzdek J, Kochaniec MK, Smolinski M, Marcinek M. Lithium polymer electrolytes for novel batteries application : the review perspective. Applied Physics A. 17 oct 2022;

52. Zheng F, Li C, Li Z, Cao X, Luo H, Liang J, et al. Advanced Composite Solid Electrolytes for Lithium Batteries: Filler Dimensional Design and Ion Path Optimization. Small. 20232;2206355.

53. McLin M, Angell CA. Contrasting conductance/viscosity relations in liquid states of vitreous and polymer solid electrolytes. J Phys Chem. avr 1988;92(8):2083‑6.

54. Zhou H, Zhao R, Xiao Y, Feng L, Yang Y, Bao L, et al. Quantum mechanical insight into the Li-ion conduction mechanism for solid polymer electrolytes. Journal of Polymer Science. 2020;58(24):3480‑7.

55. Gejji SP, Suresh CH, Babu K, Gadre SR. Ab Initio Structure and Vibrational Frequencies of (CF3SO2)2N-Li+ Ion Pairs. J Phys Chem A. 1 sept 1999;103(37):7474‑80.

56. MacGlashan GS, Andreev YG, Bruce PG. Structure of the polymer electrolyte poly(ethylene oxide)6:LiAsF6. Nature. avr 1999;398(6730):792‑4.

57. Gadjourova Z, Andreev YG, Tunstall DP, Bruce PG. Ionic conductivity in crystalline polymer electrolytes. Nature. août 2001;412(6846):520‑3.

58. Xue Z, He D, Xie X. Poly(ethylene oxide) - based electrolytes for lithium-ion batteries. Journal of Materials Chemistry A. 2015;(3,19218).

59. Druger SD, Nitzan A, Ratner MA. Dynamic bond percolation theory: A microscopic model for diffusion in dynamically disordered systems. I. Definition and one-dimensional case. The Journal of Chemical Physics. 15 sept 1983;79(6):3133‑42.

60. Ratner MA, Shriver DF. Ion transport in solvent-free polymers. Chem Rev. janv 1988;88(1):109‑24.

61. Angell CA, Liu C, Sanchez E. Rubbery solid electrolytes with dominant cationic transport and high ambient conductivity. Nature. mars 1993;362(6416):137‑9.

62. Berthier C, Gorecki W, Minier M, Armand MB, Chabagno JM, Rigaud P. Microscopic investigation of ionic conductivity in alkali metal salts-poly(ethylene oxide) adducts. Solid State Ionics. 1 sept 1983;11(1):91‑5.

63. Devaux D, Bouchet R, Glé D, Denoyel R. Mechanism of ion transport in PEO/LiTFSI complexes: Effect of temperature, molecular weight and end groups. Solid State Ionics. 29 oct 2012;227:119‑27.

64. Tominaga Y, Yamazaki K. Fast Li-ion conduction in poly(ethylene carbonate)-based electrolytes and composites filled with TiO2 nanoparticles. Chem Commun. 1 avr 2014;50(34):4448‑50.

65. Bouchet R, Phan TNT, Devaux D, Davidson P, Bertin D, Denoyel R. Charge transport in Nanostructured PS-PEO-PS triblock copolymer electrolytes. Macromolecules. 2014;47:2659‑65.

66. Gao L, Li J, Sarmad B, Cheng B, Kang W, Deng N. A 3D polyacrylonitrile nanofiber and flexible polydimethylsiloxane macromolecule combined all-solid-state composite electrolyte for efficient lithium metal batteries. Nanoscale. 9 juill 2020;12(26):14279‑89.

67. Golodnitsky D, Livshits E, Peled E. Highly conductive oriented PEO-based polymer electrolytes. Macromol Symp. oct 2003;203(1):27‑46.

68. Zhuang H, Ma W, Xie J, Liu X, Li B, Jiang Y, et al. Solvent-free synthesis of PEO/garnet composite electrolyte for highsafety all-solid-state lithium batteries. Journal of Alloys and Compounds. 2020;

69. Chen L, Li Y, Li SP, Fan LZ, Nan CW, Goodenough JB. PEO/Garnet composite electrolytes for solid-state lithium batteries : From "ceramic in polymer " to « polymer in ceramic ». Nano Energy. 2017;221‑2855.

70. Takahashi Y, Tadokoro H. Structural Studies of Polyethers, (-(CH2)m-O-)n. X. Crystal Structure of Poly(ethylene oxide). Macromolecules. 1 sept 1973;6(5):672‑5.

71. Zhang, Armand M, Rojo T. Review—Innovative Polymeric Materials for Better Rechargeable Batteries: Strategies from CIC Energigune. Journal of The Electrochemical Society. 2019;166(4):A679‑86.

72. Wookil C, Bumsang K, Ryoo WS, Earmme T. A Brief Review of Gel Polymer Electrolytes using in-situ 2 Polymerization for Lithium-ion Polymer Batteries. Polymers. 2023;15.

73. GRAY M. Polymer Electrolytes. Royal Society of Chemistry. 1997;

74. Wright PV. Developments in Polymer Electrolytes for Lithium Batteries. MRS Bull. août 2002;27(8):597‑602.

75. Xi G, Xiao M. Polymer-Based Solid Electrolytes: Material Selection, Design, and Application. Advanced Functional Materials. 2021;31.

76. Guan H yan, Lian F, Xi K, Ren Y, Sun J lin, Kumar RV. Polyvinyl formal based gel polymer electrolyte prepared using initiator free in-situ thermal polymerization method. Journal of Power Sources. 1 janv 2014;245:95‑100.

77. Wang QJ, Zhang P, Wang B, Fan LZ. A novel gel polymer electrolyte based on trimethylolpropane trimethylacrylate/ionic liquid via in situ thermal polymerization for lithium-ion batteries. Electrochimica Acta. 20 févr 2021;370:137706.

78. Yuan J, Mecerreyes D, Antonietti M. Poly(ionic liquid)s: An update. Progress in Polymer Science. juill 2013;38(7):1009‑36.

79. Chen H, Zheng M, Qian S, Ling HY, Wu Z, Liu X, et al. Functional additives for solid polymer electrolytes in flexible and high-energy-density solid-state lithium-ion batteries. Carbon Energy. 2021;3(6):929‑56.

80. Horowitz Y, Lifshitz M, Greenbaum A, Feldman Y, Greenbaum S, Sokolov AP, et al. Review—Polymer/Ceramic Interface Barriers: The Fundamental Challenge for Advancing Composite Solid Electrolytes for Li-Ion Batteries. J Electrochem Soc. 1 déc 2020;167(16):160514.

81. Eftekhari A, Saito T. Synthesis and properties of polymerized ionic liquids. European Polymer Journal. 1 mai 2017;90:245‑72.

82. Osada I, de Vries H, Scrosati B, Passerini S. Ionic-Liquid-Based Polymer Electrolytes for Battery Applications. Angew Chem Int Ed. 11 janv 2016;55(2):500‑13.

83. Guo P, Su A, Wei Y, Liu X, Li Y, Guo F, et al. Healable, Highly Conductive, Flexible, and Nonflammable Supramolecular Ionogel Electrolytes for Lithium-Ion Batteries. ACS Appl Mater Interfaces. 29 mai 2019;11(21):19413‑20.

84. Yoon HK, Chung WS, Jo NJ. Study on ionic transport mechanism and interactions between salt and polymer chain in PAN based solid polymer electrolytes containing LiCF3SO3. Electrochimica Acta. nov 2004;50(2‑3):289‑93.

85. Yi C, Liu W, Li L, Dong H, Liu J. Polymer-in-salt solid electrolytes for lithium-ion batteries. Functional Materials Letters. 2019;

86. Wu B, Wang L, Li Z, Zhao M, Chen K, Liu S, et al. Performance of “Polymer-in-Salt” Electrolyte PAN-LiTFSI Enhanced by Graphene Oxide Filler. J Electrochem Soc. 12 août 2016;163(10):A2248.

87. Aldalur I, Martinez-Ibañez M, Piszcz M, Rodriguez-Martinez LM, Zhang H, Armand M. Lowering the operational temperature of all-solid-state lithium polymer cell with highly conductive and interfacially robust solid polymer electrolytes. Journal of Power Sources. avr 2018;383:144‑9.

88. Martinez-Ibanez M, Sanchez-Diez E, Qiao L, Zhang Y, Judez X, Santiago A, et al. Unprecedented improvement of Single Li ion conductive Solid Polymer Electrolyte through Salt Additive. Advanced Functional Materials. 2020;30(2000455).

89. Chen G, Niu C, Chen Y, Shang W, Qu Y, Du Z, et al. A single-ion conducting polymer electrolyte bases on poly(lithium 4-styrenesulfonate) for high-performance lithium metal batteries. Solid State Ionics. 2019;341(115048):0167‑2738.

90. Zeyu Li, Feng Liu, Shaoshan Chen, Fei Zhai, Yu Li, Yiyu Feng, Wei Feng. Single Li ion conducting SPE based on Carbon Quantum Dots for Li-metal batteries. Nano Energy. 2020;82(105698):2211‑855.

91. Aldalur I, Martinez-Ibañez M, Piszcz M, Zhang H, Armand M. Self-Standing Highly Conductive Solid Electrolytes Based on Block Copolymers for Rechargeable All-Solid-State Lithium-Metal Batteries. Batteries & Supercaps. 2018;(1):149‑59.

92. Devaux D, Glé D, Phan TNT, Gigmes, Giroud E, Deschamps M, et al. Optimization of Block Copolymer elecrtolytes for Li Metal batteries. Chemistry of Materials. 2015;(27):4682‑92.

93. Zhang H, Chen Y, Li C, Armand M. Electrolyte and anode-electrolyte interphase in solid-state lithium metal polymer batteries: A perspective. SusMat. 2021;(1):1‑14.

94. Zaheer M, Xu H, Wang B, Li L, Deng Y. An In Situ Polymerized Comb-Like PLA/PEG-based Solid Polymer Electrolyte for Lithium Metal Batteries. J Electrochem Soc. 4 déc 2019;167(7):070504.

95. Mackanic DG, Michaels W, Lee M, Feng D, Lopez J, Qin J, et al. Crosslinked Poly(tetrahydrofuran) as a Loosely Coordinating Polymer Electrolyte. Advanced Energy Materials. 2018;8(25):1800703.

96. Porcarelli L, Gerbaldi C, Bella F, Nair JR. Super Soft All-Ethylene Oxide Polymer Electrolyte for Safe All-Solid Lithium Batteries. Sci Rep. 21 janv 2016;6(1):19892.

97. Judez X, Zhang H, Li C, Eshetu GG, Zhang Y, González-Marcos JA, et al. Polymer-Rich Composite Electrolytes for All-Solid-State Li–S Cells. J Phys Chem Lett. 3 août 2017;8(15):3473‑7.

98. Fu K (Kelvin), Gong Y, Dai J, Gong A, Han X, Yao Y, et al. Flexible, solid-state, ion-conducting membrane with 3D garnet nanofiber networks for lithium batteries. Proceedings of the National Academy of Sciences. 28 juin 2016;113(26):7094‑9.

99. Bae J, Li Y, Zhao F, Zhou X, Ding Y, Yu G. Designing 3D nanostructured garnet frameworks for enhancing ionic conductivity and flexibility in composite polymer electrolytes for lithium batteries. Energy Storage Materials. 1 nov 2018;15:46‑52.

100. Jeong K, Park S, Jung GY, Kim SH, Lee YH, Kwak SK, et al. Solvent-Free, Single Lithium-Ion Conducting Covalent Organic Frameworks. J Am Chem Soc. 10 avr 2019;141(14):5880‑5.

101. Meng N, Zhu X, Lian F. Particles in composite polymer electrolyte for solid-state lithium batteries: A review | Elsevier Enhanced Reader. Particuology. 2021;60:1674‑2001.

102. Kuhnert E, Ladenstein L, Jodlbauer A, Slugovc C, Trimmel G, Wilkening HMR, et al. Lowering the Interfacial Resistance in Li6.4La3Zr1.4Ta0.6O12|Poly(Ethylene Oxide) Composite Electrolytes | Elsevier Enhanced Reader. Cell reports Physical science [Internet]. 2020;1. Disponible sur: https://reader.elsevier.com/reader/sd/pii/S2666386420302290

103. Kim A, Woo S, Kang M, Park H, Kang B. Research Progresses of Garnet-Type Solid Electrolytes for Developing All-Solid-State Li Batteries. Frontiers in Chemistry [Internet]. 2020 [cité 19 janv 2023];8. Disponible sur: https://www.frontiersin.org/articles/10.3389/fchem.2020.00468

104. Feng J, Wang L, Chen Y, Wang P, Zhang H, He X. PEO based polymer-ceramic hybrid solid electrolytes: a review. Nano Convergence. 10 janv 2021;8(1):2.

105. Bidal J, Cézard C, Bouvier B, Hadad C, Nguyen Van Nhien A, Becuwe M. Fundamental insight into the interaction between a lithium salt and an inorganic filler for ion mobility using a synergic theoretical-experimental approach. Journal of Colloid and Interface Science. 1 nov 2022;625:734‑42.

106. Croce F, Persi L, Scrosati B, Serraino-Fiory F, Plichta E, Hendrickson MA. Role of the ceramic fillers in enhancing the transport properties of composite polymer electrolytes. Electrochimica Acta. 1 mai 2001;46(16):2457‑61.

107. Zhang J, Zhao N, Zhang M, Li Y, Chu PK, Guo X, et al. Flexible and ion-conducting membrane electrolytes for solid-state lithium batteries: Dispersion of garnet nanoparticles in insulating polyethylene oxide. Nano Energy. 1 oct 2016;28:447‑54.

108. Liu W, Liu N, Sun J, Hsu PC, Li Y, Lee HW, et al. Ionic Conductivity Enhancement of Polymer Electrolytes with Ceramic Nanowire Fillers. Nano Lett. 8 avr 2015;15(4):2740‑5.

109. Palmer MJ, Kalnaus S, Dixit MB, Westover AS, Hatzell KB, Dudney NJ, et al. A three-dimensional interconnected polymer/ceramic composite as a thin film solid electrolyte. Energy Storage Materials. 1 avr 2020;26:242‑9.

110. Xu Z, Yang T, Chu X, Su H, Wang Z, Chen N, et al. Strong Lewis Acid–Base and Weak Hydrogen Bond Synergistically Enhancing Ionic Conductivity of Poly(ethylene oxide)@SiO2 Electrolytes for a High Rate Capability Li-Metal Battery. ACS Appl Mater Interfaces. 4 mars 2020;12(9):10341‑9.

111. Zhen L, Ammar MA, Xiaowei L, Yangxing L, Zhiping L. Scalable fabrication of Solvent-Free composite solid electrolyte by a continuous thermal extrusion process. 2022;

112. Yu X, Zhai P, Zhao N, Guo X. In-Situ Plasticized LLZTO-PVDF Composite Electrolytes for High-Performance Solid-State Lithium Metal Batteries. Batteries. mai 2023;9(5):257.

113. Guo J, Zheng J, Zhang W, Lu Y. Recent Advances of Composite Solid-State Electrolytes for Lithium-Based Batteries. Energy Fuels. 15 juill 2021;35(14):11118‑40.

114. Yuan C, Li J, Han P, Lai Y, Zhang Z, Liu J. Enhanced electrochemical performance of poly(ethylene oxide) based composite polymer electrolyte by incorporation of nano-sized metal-organic framework. Journal of Power Sources. 15 oct 2013;240:653‑8.

115. Das S, Ghosh A. Ion conduction and relaxation in PEO-LiTFSIAl2O3 polymer nanocomposite electrolytes. journal of applied physics. 2015;117(174103).

116. Zhan H, Wu M, Wang R, Wu S, Li H, Tian T, et al. Excellent Performances of Composite Polymer Electrolytes with Porous Vinyl-Functionalized SiO2 Nanoparticles for Lithium Metal Batteries. Polymers. janv 2021;13(15):2468.

117. Li X, Yang L, Shao D, Luo K, Liu L, Wu Z, et al. Preparation and application of poly(ethylene oxide)-based all solid-state electrolyte with a walnut-like SiO2 as nano-fillers. Journal of Applied Polymer Science. 2020;137(24):48810.

118. Choudhury S, Mangal R, Agrawal A, Archer LA. A highly reversible room-temperature lithium metal battery based on crosslinked hairy nanoparticles. Nat Commun. 4 déc 2015;6(1):10101.

119. Lin D, Liu W, Liu Y, Lee HR, Hsu PC, Liu K, et al. High Ionic Conductivity of Composite Solid Polymer Electrolyte via In Situ Synthesis of Monodispersed SiO2 Nanospheres in Poly(ethylene oxide). Nano Lett. 13 janv 2016;16(1):459‑65.

120. Liang J, Luo J, Sun Q, Yang X, Li R, Sun X. Recent progress on solid-state hybrid electrolytes for solid-state lithium batteries | Elsevier Enhanced Reader. Energy Storage Materials. 2019;21:308‑34.

121. Zhao CZ, Zhang XQ, Cheng XB, Zhang R, Xu R, Chen PY, et al. An anion-immobilized composite electrolyte for dendrite-free lithium metal anodes. Proceedings of the National Academy of Sciences. 17 oct 2017;114(42):11069‑74.

122. Thangadurai V, Narayanan S, Pinzaru D. Garnet-type solid-state fast Li ion conductors for Li batteries: critical review. Chem Soc Rev. 9 juin 2014;43(13):4714‑27.

123. Li Y, Han JT, Wang CA, Xie H, Goodenough JB. Optimizing Li+ conductivity in a garnet framework. J Mater Chem. 10 juill 2012;22(30):15357‑61.

124. Ren Y, Liu T, Shen Y, Lin Y, Nan CW. Chemical compatibility between garnet-like solid state electrolyte Li6.75La3Zr1.75Ta0.25O12 and major commercial lithium battery cathode materials. Journal of Materiomics. 1 sept 2016;2(3):256‑64.

125. Zheng J, Wang P, Liu H, Hu YY. Interface-Enabled Ion Conduction in Li10GeP2S12–Poly(ethylene Oxide) Hybrid Electrolytes. ACS Appl Energy Mater. 25 févr 2019;2(2):1452‑9.

126. Song YW, Heo K, Lee J, Hwang D, Kim MY, Kim SJ, et al. Lithium-ion transport in inorganic active fillers used in PEO-based composite solid electrolyte sheets. RSC Advances. 2021;11(51):31855‑64.

127. Zheng J, Hu YY. New Insights into the Compositional Dependence of Li-Ion Transport in Polymer–Ceramic Composite Electrolytes. ACS Appl Mater Interfaces. 31 janv 2018;10(4):4113‑20.

128. Gupta A, Sakamoto J. Controlling Ionic Transport through the PEO-LiTFSI/LLZTO Interface. Electrochem Soc Interface. 1 janv 2019;28(2):63.

129. Pan K, Zhang L, Qian W, Wu X, Dong K, Zhang H, et al. A Flexible Ceramic/Polymer Hybrid Solid Electrolyte for Solid-State Lithium Metal Batteries. Advanced Materials. 2020;32(17):2000399.

130. Huang Z, Pang W, Liang P, Jin Z, Grundish N, Li Y, et al. A dopamine modified Li6.4La3Zr1.4Ta0.6O12/PEO solid-state electrolyte: enhanced thermal and electrochemical properties. J Mater Chem A. 9 juill 2019;7(27):16425‑36.

131. Kim HK, Barai P, Chavan K, Srinivasan V. Transport and mechanical behavior in PEO-LLZO composite electrolytes. J Solid State Electrochem. 1 sept 2022;26(9):2059‑75.

132. Zhang M, Pan P, Cheng Z, Mao J, Jiang L, Ni C, et al. Flexible, Mechanically Robust, Solid-State Electrolyte Membrane with Conducting Oxide-Enhanced 3D Nanofiber Networks for Lithium Batteries. Nano Lett. 25 août 2021;21(16):7070‑8.

133. Venkataraman N, Rangarajan S, Matthewson MJ, Harper B, Safari A, Danforth SC, et al. Feedstock material property – process relationships in fused deposition of ceramics (FDC). Rapid Prototyping Journal. 1 janv 2000;6(4):244‑53.

134. Zhang J, Feng X, Patil H, Tiwari RV, Repka MA. Coupling 3D printing with hot-melt extrusion to produce controlled-release tablets. International Journal of Pharmaceutics. 15 mars 2017;519(1):186‑97.

135. Go J, Schiffres SN, Stevens AG, Hart AJ. Rate limits of additive manufacturing by fused filament fabrication and guidelines for high-throughput system design. Additive Manufacturing. 1 août 2017;16:1‑11.

136. BERAN T, Mulholland T, Henning F, Rudolph N, Osswald TA. Nozzle clogging factors during fused filament fabrication of spherical particle filled polymer. Additive Manufacturing. 2018;23:206‑14.

137. Arrigo R, Frache A. FDM Printability of PLA Based-Materials: The Key Role of the Rheological Behavior. Polymers. janv 2022;14(9):1754.

138. Xu P, Li J, Meda A, Osei-Yeboah F, Peterson ML, Repka M, et al. Development of a quantitative method to evaluate the printability of filaments for fused deposition modeling 3D printing | Elsevier Enhanced Reader. International Journal of Pharmaceutics [Internet]. 2020;588(119760). Disponible sur: https://reader.elsevier.com/reader/sd/pii/S0378517320307444

139. Samaro A, Shaqour B, Goudarzi NM, Ghijs M, Cardon L, Boone MN, et al. Can filaments, pellets and powder be used as feedstock to produce highly drug-loaded ethylene-vinyl acetate 3D printed tablets using extrusion-based additive manufacturing? International Journal of Pharmaceutics. 25 sept 2021;607:120922.

140. Vaes D, Van Puyvelde P. Semi-crystalline feedstock for filament-based 3D printing of polymers. Progress in Polymer Science. 1 juill 2021;118:101411.

141. Tian X, Todoroki A, Liu T, Wu L, Hou Z, Ueda M, et al. 3D Printing of Continuous Fiber Reinforced Polymer Composites: Development, Application, and Prospective. Chinese Journal of Mechanical Engineering: Additive Manufacturing Frontiers. 1 mars 2022;1(1):100016.

142. Daurskikh A, Sgambati A, Graça D, Berg M, Baptista A, Angelo M, et al. Influence of spatial orientation on properties of 3D printed PEEK parts and their design adaptation. In Bremen, Germany; 2018. Disponible sur: https://www.scopus.com/inward/record.uri?eid=2-s2.0-85065306926&partnerID=40&md5=8b37a3ec09517fdbba31d221393d7751

143. Prater T, Werkheiser MJ, Ledbetter F, Morgan K. In-Space Manufacturing at NASA Marshall Space Flight Center: A Portfolio of Fabrication and Recycling Technology Development for the International Space Station. In Orlando: American Institute of Aeronautics and Astronautics; 2018 [cité 15 sept 2023]. (AIAA SPACE Forum). Disponible sur: https://arc.aiaa.org/doi/10.2514/6.2018-5364

144. Made In Space. Additive Manufacturing Facility (AMF) User Guide [Internet]. 2016. Disponible sur: https://www.eisacademy.org/pluginfile.php/1437/mod_resource/content/3/AMF%20User%20Guide.pdf

145. Risdon D. In-Space Manufacturing (ISM) ISS Refabricator Technology Demonstration. Recycling and Sustainable Acquisition (RSA) Workshop [Internet]. mai 2019;No. MSFC-E-DAA-TN68285. Disponible sur: https://ntrs.nasa.gov/api/citations/20190005004/downloads/20190005004.pdf

146. Daurskikh A, Sgambati A, Teixeira P, Silva R, Facciolati L, Lallemand E, et al. Quality of AM polymer parts produced using a printer without build volume constraint in space environment. In Virtual; 2021.

147. Shireman K. ISS Safety Requirements Document - SSP 51721. 2019;National Aeronautics and Space Administration International Space Station Program Johnson Space Center.

148. Or D, Tuller M, Jones SB. Liquid Behavior in Partially Saturated Porous Media under Variable Gravity. Soil Science Society of America Journal. 2009;73(2):341‑50.

149. Duty C, Ajinjeru C, Kishore V, Compton B, Hmeidat N, Chen X, et al. What makes a material printable? A viscoelastic model for extrusion-based 3D printing of polymers. Journal of Manufacturing Processes. 1 oct 2018;35:526‑37.

150. Maurel A, Courty M, Fleutot B, Tortajada H, Prashantha K, Armand M, et al. Highly Loaded Graphite–Polylactic Acid Composite-Based Filaments for Lithium-Ion Battery Three-Dimensional Printing. Chem Mater. 13 nov 2018;30(21):7484‑93.

151. Verdier N, Foran G, Lepage D, Prébé A, Aymé-Perrot D, Dollé M. Challenges in Solvent-Free Methods for Manufacturing Electrodes and Electrolytes for Lithium-Based Batteries. Polymers. 2021;(13):323.

152. Yang C, Tian X, Li D, Cao Y, Zhao F, Shi C. Influence of thermal processing conditions in 3D printing on the crystallinity and mechanical properties of PEEK material. Journal of Materials Processing Technology. 1 oct 2017;248:1‑7.

153. Li XR, Guo J, LI WD, Zhang LY, Wang C, Guo BH, et al. Analysis of Morphology and Electrical Insulation of 3D Printing Parts. In: 2018 IEEE International Conference on High Voltage Engineering and Application (ICHVE). 2018. p. 1‑4.

154. Pötschke P, Paul DR. Formation of Co-continuous Structures in Melt-Mixed Immiscible Polymer Blends. Journal of Macromolecular Science. 2003;Part C: Polymer Reviews(43:1):87‑141.

155. Plattier J, Benyahia L, Dorget M, Niepceron F, Tassin JF. Viscosity-induced filler localisation in immiscible polymer blends. Polymer. 24 févr 2015;59:260‑9.

156. Meija A, García N, Guzman J, Tiemblo P. Thermoplastic and solid-like electrolytes with liquid-like ionic conductivity based on poly(ethylene oxide) nanocomposites. Solid State Ionics. 2014;261:74‑80.

157. Meija A, Devaraj S, Guzman J, Lopez del Amo JM, García N, Rojo T, et al. Scalable plasticized polymer electrolytes reinforced with surface modified sepiolite fillers : A feasibility study in lithium metal polymer batteries. Journal of Power Sources. 2016;306:772‑8.

158. Aldalur I, Zhang H, Piszcz M, Oteo U, Rodriguez-Martinez LM, Shanmukaraj D, et al. Jeffamine based polymers as higly conductive polymer electrolytes and cathode binder matéreilas for battery application. Journal of Power Sources. 2017;347:37‑46.